Since January 2020 Elsevier has created a COVID-19 resource centre with free information in English and Mandarin on the novel coronavirus COVID-19. The COVID-19 resource centre is hosted on Elsevier Connect, the company's public news and information website.

Elsevier hereby grants permission to make all its COVID-19-related research that is available on the COVID-19 resource centre - including this research content - immediately available in PubMed Central and other publicly funded repositories, such as the WHO COVID database with rights for unrestricted research re-use and analyses in any form or by any means with acknowledgement of the original source. These permissions are granted for free by Elsevier for as long as the COVID-19 resource centre remains active.

Cell Reports
Methods

Report

Unlocking SARS-CoV-2 detection in low- and middle-income countries

Graphical abstract

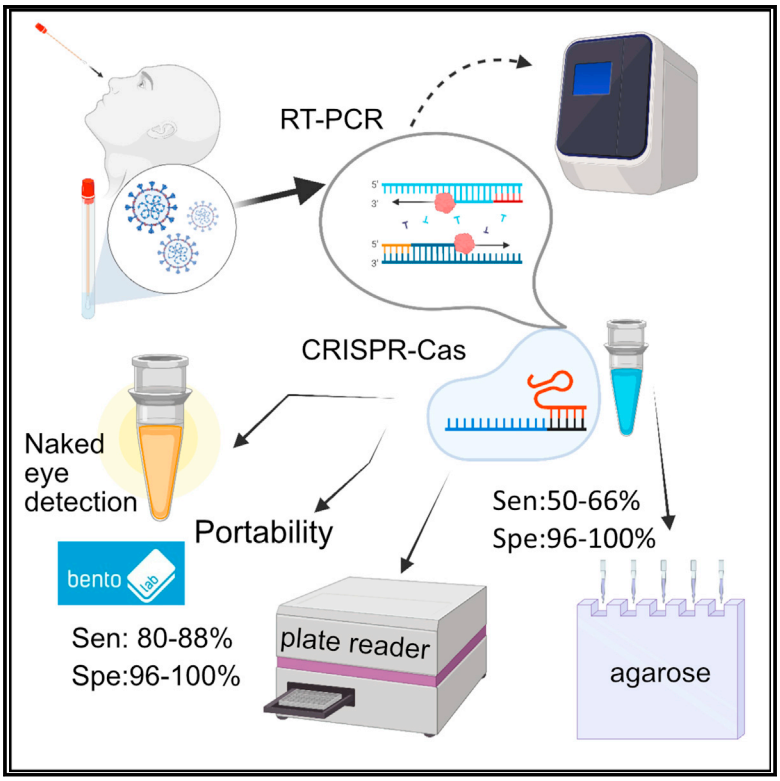

Highlights

- Molecular detection of SARS-CoV-2 using RT-PCR coupled to CRISPR-Cas12a
- A validated method that accounts for LMICs' infrastructure limitations
- Compatibility with a portable molecular laboratory to reach remote locations
- The test uses locally produced enzymes and open-source options to visualize results

Authors

Roberto Alcántara, Katherin Peñaranda, Gabriel Mendoza-Rojas, ..., Juana del Valle-Mendoza, Vanessa Adaui, Pohl Milón

Correspondence

pmilon@upc.edu.pe

In brief

Alcántara et al. present an open-source SARS-CoV-2 molecular test that uses locally produced reagents. High sensitivity and specificity were observed for middle and high viral load samples. The assay is compatible with portable molecular systems, allowing its implementation in underequipped and remote communities.

Alcántara et al., 2021, Cell Reports Methods *1*, 100093
November 22, 2021 © 2021 The Author(s).
https://doi.org/10.1016/j.crmeth.2021.100093

CellPress

Please cite this article in press as: Alcántara et al., Unlocking SARS-CoV-2 detection in low- and middle-income countries, Cell Reports Methods (2021), https://doi.org/10.1016/j.crmeth.2021.100093

Cell Reports Methods

CellPress
OPEN ACCESS

Report

Unlocking SARS-CoV-2 detection in low- and middle-income countries

Roberto Alcántara,[1] Katherin Peñaranda,[1] Gabriel Mendoza-Rojas,[1] Jose A. Nakamoto,[1] Johanna Martins-Luna,[1,2] Juana del Valle-Mendoza,[1,2] Vanessa Adaui,[1] and Pohl Milón[1,3,*]
[1]Centre for Research and Innovation, Health Sciences Faculty, Universidad Peruana de Ciencias Aplicadas (UPC), Lima 15023, Peru
[2]Laboratorio de Biología Molecular, Instituto de Investigación Nutricional, Lima, Peru
[3]Lead contact
*Correspondence: pmilon@upc.edu.pe
https://doi.org/10.1016/j.crmeth.2021.100093

MOTIVATION The COVID-19 pandemic has brought to light limitations of the public health infrastructure in LMICs, namely, limited capacity for molecular test development, absence of policies and regulations, and underdeveloped biotechnological industries certified for good manufacturing practices. These limitations were accentuated by the global demand for molecular diagnostics, which further stressed the detection and diagnostic capabilities of LMICs. The lack of molecular testing precluded proper tracing and isolation of infectious individuals, contributing to the highest numbers of cases per habitant reported. Thus, LMICs' government surveillance and containment measures lacked appropriate tools for timely pandemic control. In contrast, research laboratories are more widely available in LMICs, providing a strategic source of infrastructure and qualified professionals. The molecular toolkit reported here aims to exploit available laboratory setups in an attempt to cope with the above limitations that COVID-19 unmasked in LMICs.

SUMMARY

Low- and middle-income countries (LMICs) are significantly affected by SARS-CoV-2, partially due to their limited capacity for local production and implementation of molecular testing. Here, we provide detailed methods and validation of a molecular toolkit that can be readily produced and deployed using laboratory equipment available in LMICs. Our results show that lab-scale production of enzymes and nucleic acids can supply over 50,000 tests per production batch. The optimized one-step RT-PCR coupled to CRISPR-Cas12a-mediated detection showed a limit of detection of 10^2 ge/μL in a turnaround time of 2 h. The clinical validation indicated an overall sensitivity of 80%–88%, while for middle and high viral load samples (Cq $\leq$ 31) the sensitivity was 92%–100%. The specificity was 96%–100% regardless of viral load. Furthermore, we show that the toolkit can be used with the mobile laboratory Bento Lab, potentially enabling LMICs to implement detection services in unattended remote regions.

INTRODUCTION

SARS-CoV-2 has infected more than 113 million people and caused 2,526,007 deaths worldwide, forcing countries to adopt strict quarantine measures to control the contagion (as of March 2021, WHO, 2021). This has negatively affected local and global economies, with more than trillions of dollars in economic loss (Ibn-Mohammed et al., 2021). Since the beginning of the COVID-19 pandemic, early detection of the virus appeared necessary to restrict the rate of transmission, extremely high for SARS-CoV-2. High-income countries (HICs) implemented massive molecular testing facilities together with contact tracing technologies and proper isolation of positive patients (Ferretti et al., 2020; Kucharski et al., 2020). Consequently, the scale of the pandemic outbreak generated an unprecedented high demand for molecular testing equipment and materials, precluding their access in low- and middle-income countries (LMICs) (Figure 1A). The shortage of viral RNA extraction kits, quantitative reverse-transcription polymerase chain reaction (qRT-PCR) materials, and instrumentation limited the capability of LMICs to accurately identify carriers of the virus (Adepoju, 2020; Rubin et al., 2020). Both the lack of molecular testing and the high rate of viral propagation created a perfect storm for LMICs (Abbott et al., 2020). Countries such as Brazil, Argentina, Colombia, and Peru, among others, surpassed developed countries in the numbers of both infections and deaths per population (Roser and Ortiz-Ospina, 2021; Hasell et al., 2020). Consequently, there is a high need to provide LMICs with tools for SARS-CoV-2

This is an open access article under the CC BY-NC-ND license (http://creativecommons.org/licenses/by-nc-nd/4.0/).

Please cite this article in press as: Alcántara et al., Unlocking SARS-CoV-2 detection in low- and middle-income countries, Cell Reports Methods (2021), https://doi.org/10.1016/j.crmeth.2021.100093

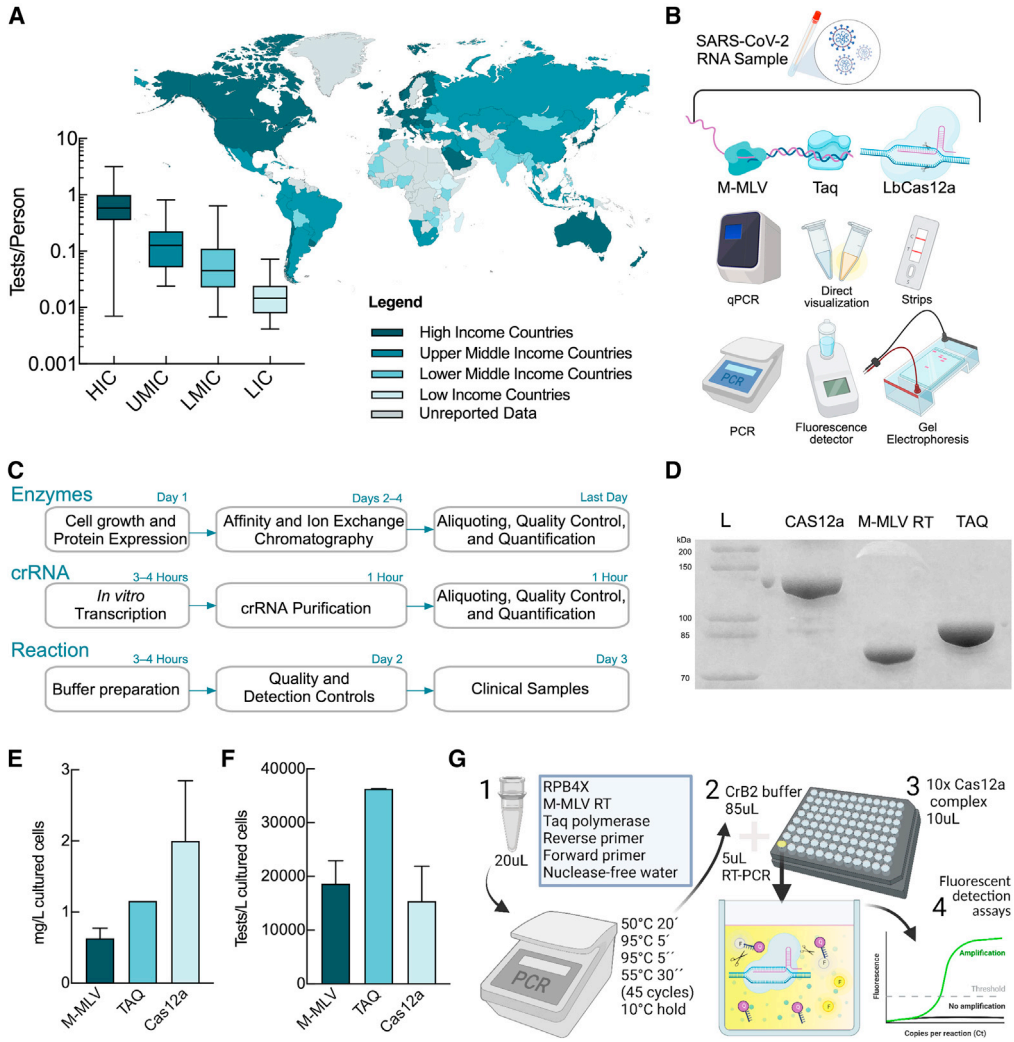

Figure 1. SARS-CoV-2 testing availability, inequality, and local production of reagents

(A) Molecular testing availability as a function of income classification of countries by the World Bank. Total tests per thousand inhabitants were obtained from OurWorldInData.org (Hasell et al., 2020). The country classification map was done using mapchart.net.

(B) Current molecular diagnostic platforms for detection of SARS-CoV-2.

(C) Production scheme for recombinant DNA polymerases Taq and M-MLV, LbCas12a nuclease, and crRNAs.

(D) Recombinant enzyme visualization and purity evaluation by SDS-PAGE 10%.

(E) Comparison of enzyme yield expressed as milligrams of pure protein produced in 1 L of bacterial cell culture.

(F) Estimated total test (reverse transcription, PCR, or CRISPR-Cas12a) reactions achievable in 1 L of bacterial cell culture producing recombinant enzymes M-MLV reverse transcriptase (RT), Taq DNA polymerase, or LbCas12a, respectively, out of *E. coli*.

(G) Schematics and optimized conditions for the method presented here. The viral RNA is amplified by RT-PCR (step 1) and used for CRISPR-Cas12a-mediated detection (steps 2 to 4). Cas12a, upon recognition of the amplified target DNA, activates its collateral activity for ssDNA cleavage. The reaction mixture contains a dual-labeled ssDNA reporter probe, with fluorescein and a quencher. Upon Cas12a-dependent cleavage, the fluorescence of the fluorophore increases due to quencher diffusion (step 3). Error bars in (E) and (F) show the standard error, while in (A) they indicate the minimum and maximum.

detection, with the aim to decrease their dependence on the international supply.

In addition to the high demand for biotechnological supplies, LMICs have limited infrastructure, laboratory equipment, and trained professionals. This is further evidenced in geographical regions that are distant from major capital cities. Several new methods have been recently reported, using qRT-PCR (Corman et al., 2020), loop-mediated isothermal amplification (LAMP; Hu et al., 2020), and CRISPR-Cas (Hou et al., 2020), among others (Figure 1B). Despite their potential for coping with LMICs' limitations being high, a concrete solution is yet unavailable. qRT-PCR requires real-time thermocyclers that are costly and not readily available. Although LAMP-based methods require basic laboratory equipment, and local production of enzymes is reported, their deployment in LMICs remains limited (Alekseenko et al., 2021; Ali et al., 2020; Bhadra et al., 2020; Kellner et al., 2020;

Matute et al., 2021; Sherrill-Mix et al., 2021). CRISPR-based methods are still not widely used worldwide, although several proofs of concept are available (Broughton et al., 2020; Hou et al., 2020; Metsky et al., 2020).

The CRISPR-Cas systems include a DNA/RNA nuclease (i.e., Cas enzyme family) and its programmable CRISPR RNA (crRNA) (Chen and Doudna, 2017; Jinek et al., 2012). The specificity of the CRISPR-Cas system depends on the crRNA sequence, which binds with a high specificity to the complementary target nucleic acid. CRISPR-Cas systems can even differentiate at the one-base level (Huang et al., 2018; Pardee et al., 2016). Cas12a is a member of the Cas family that targets double-stranded DNA (dsDNA) (Zetsche et al., 2015). In addition to the principal dsDNA nuclease activity (*cis*-cleavage), Cas12a reports an indiscriminate *trans*-cleavage activity on single-stranded DNA (ssDNA) (Chen et al., 2018). This activity has been reported for other Cas enzymes, such as Cas13 (Gootenberg et al., 2017) and Cas14 (Harrington et al., 2018). Once the target has been recognized by matching with the crRNA, the Cas12a nuclease is activated and shows a *trans*-cleavage activity. This non-specific ssDNase activity degrades both linear and circular ssDNA molecules (Chen et al., 2018). CRISPR-Cas diagnostic tests take advantage of the use of a double-labeled ssDNA as a fluorescent reporter. Like TaqMan probes, the ssDNA reporter probe contains a quencher and fluorophore that will generate a fluorescent signal only when it is cleaved by an activated Cas enzyme upon target recognition. Different diagnostic methods based on CRISPR-Cas systems have been reported (i.e., DETECTR (Chen et al., 2018), HOLMES (Li et al., 2019; Li et al., 2019), and SHERLOCK (Gootenberg et al., 2017). Available CRISPR-based methods can be put into two categories: detection after amplification of the genetic material and direct detection by the CRISPR-Cas complex (Fozouni et al., 2021). Detection after amplification of the genetic material can also be divided into two categories depending on the amplification method: isothermal (LAMP or recombinase polymerase amplification [RPA]) (Hu et al., 2020; Joung et al., 2020; Sun et al., 2021; Wang et al., 2020) or thermal cycling (reverse transcription plus PCR) (Huang et al., 2020). Thus, CRISPR-Cas provides a versatile tool for detecting the amplified genetic material from SARS-CoV-2.

Here, we describe a molecular toolkit that can be readily produced and deployed in LMICs using minimal and broadly available laboratory equipment (Figure 1B). Together with detailed protocols for the production of biologicals and step-by-step optimization (Figure 1C), we provide a clinical performance evaluation for SARS-CoV-2 detection. Altogether, we sought to alleviate the reduced availability of molecular detection methods that affect LMICs in the control of the COVID-19 pandemic (Figure 1A).

RESULTS

Local production of key biological components

The current pandemic situation caused by SARS-CoV-2 has revealed the vast number of limitations of LMIC health systems. In response to this need, we first validated and adapted open-source protocols for the local production of biological reagents using minimal laboratory equipment in LMICs, focusing on versatile and widely used enzymes, namely the Taq DNA polymerase and M-MLV reverse transcriptase (M-MLV RT), for nucleic acid amplification (Figure 1C). Some of the methods in our toolkit use the LbCas12a (herein called Cas12a) enzyme for CRISPR-Cas-mediated detection. Thus, we also describe the production of Cas12a together with the required CRISPR guide RNAs (crRNA) in an LMIC setup (Figure S1).

Each required enzyme was produced to high purity following a 4-day scheme (Figure 1C). On day 1, *E. coli* BL21(DE3) carrying the respective expression plasmid (STAR Methods key resources table) was grown in Luria-Bertani medium (typically 1–4 L) using antibiotic selection throughout the process. Protein induction was achieved by the addition of isopropyl β-D-1-thiogalactopyranoside (IPTG). Typically, 3–5 g of dry cells was obtained for each liter of cell culture. Days 2 and 3 involved purification steps, which can be carried out manually or in a scaling-up stage using liquid chromatography equipment (fast protein liquid chromatography [FPLC] or high-performance liquid chromatography [HPLC]) if available. Typically, 6–12 mL of enzymes is obtained and stored. The final day is dedicated to enzyme quantification and characterization through gel imaging and spectrophotometry, preparation of aliquots, and storage of the produced enzymes at low temperatures (−20°C to −80°C) (Figure 1C, detailed protocols are available in STAR Methods). The standardized protocols showed high purity and yields of the enzymes (Figures 1D–1F). Average purity ranged between 90% and 99%, comparable to or higher than commercial counterparts (Figure 1D). The protein production yield unlocks between 20,000 and 40,000 RT-PCRs per liter of cell culture (Figure 1F). The production of Cas12a allows around 20,000 CRISPR-Cas reactions per liter of cell culture. As seen in Figure 1E, Cas12a presents the highest yield, with 2 mg/L cells, followed by Taq DNA polymerase, with 1.2 mg/L cells, and finally, M-MLV RT, with 0.6 mg/L cells. However, due to the difference in working concentrations, Taq allows the highest number of reactions per liter of cell culture.

In general, upscaling the production process to 4 L cell culture allows enzyme production for 160,000 PCRs, 80,000 retro-transcription reactions, and 60,000 CRISPR-Cas12a reactions. crRNAs can also be produced locally from synthetic dsDNA templates (Table S1) using commercially available *in vitro* transcription kits (STAR Methods key resources table). crRNA production and purification from a 40 μL reaction yielded on average 340 μg of *in vitro*-transcribed crRNA, accounting for more than 16,000 CRISPR-Cas12a-mediated detection reactions. Altogether, the methods described in detail are compatible with the timely production of all key components for molecular detection of SARS-CoV-2 in a minimal laboratory setup (Figure 1G) (STAR Methods).

Target selection

Currently, nucleic acid amplification tests (NAAT) are considered the recommended, most sensitive tests for SARS-CoV-2 detection (Böger et al., 2021; Kevadiya et al., 2021). qRT-PCR is the gold standard molecular test (Corman et al., 2020), and different targets at the ORF1ab, S, E, or N gene have been reported for molecular detection (Broughton et al., 2020; Esbin et al., 2020; Huang et al., 2020; Javalkote et al., 2020). Differences in specificity, amplification efficiency, and also downstream detection

Please cite this article in press as: Alcántara et al., Unlocking SARS-CoV-2 detection in low- and middle-income countries, Cell Reports Methods (2021), https://doi.org/10.1016/j.crmeth.2021.100093

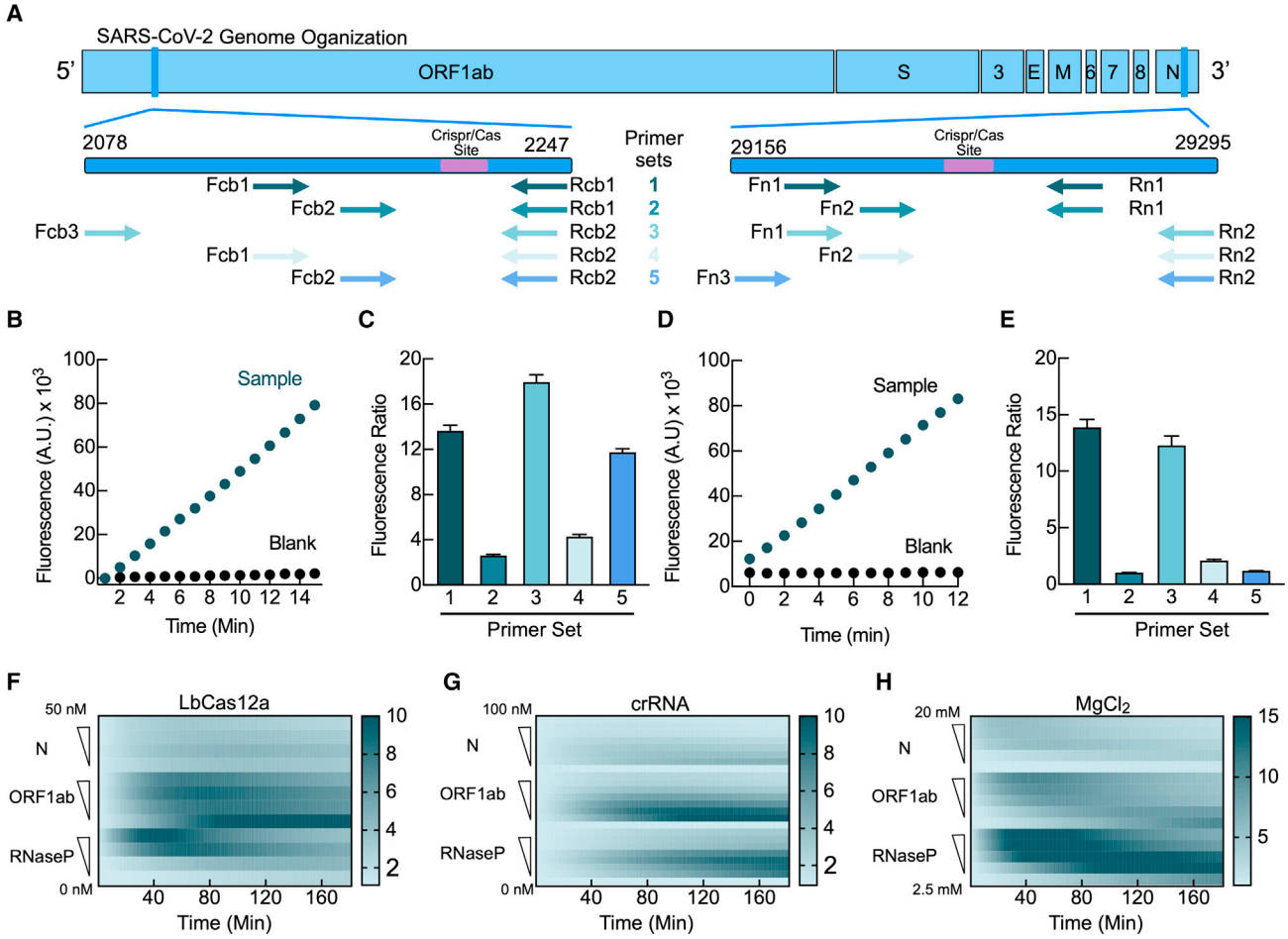

Figure 2. Optimization of SARS-CoV-2 *loci* amplification by RT-PCR and CRISPR-Cas-mediated detection

(A) Schematic representation of the SARS-CoV-2 genome and primer localization for ORF1ab and N target genes. Sequences matched by the crRNAs are highlighted (violet box) in the schematic representations of the amplified regions, for the ORF1ab (nucleotide positions 2,190–2,210) and N (nucleotide positions 29,195–29,214) targets.

(B) Example fluorescence time course of CRISPR-Cas12a-mediated recognition of ORF1ab using primer set 3.

(C) Fluorescence ratios comparing five primer combinations for ORF1ab. Colors for the primer combinations are as in (A).

(D) Same as (B) for the N detection *locus*.

(E) Comparison of five primer combinations for the N detection region.

(F–H) Heatmaps displaying the CRISPR-Cas12a reaction components that were optimized, namely LbCas12a (F), crRNA (G), and magnesium (H), for both viral detection *loci* and the human RNaseP sample control. Reaction fluorescence ratios are depicted with continuous color shading. The concentrations of Cas12a, crRNA, and magnesium were 10 nM, 15 nM, and 10 mM, respectively, unless it was the variable under study. Fluorescence ratio is defined as the fluorescence of the test sample over that of the RT-PCR non-template control (blank) at a given time. Error bars represent the standard deviation of at least three independent measurements.

(i.e., CRISPR-Cas) have been described (Joung et al., 2020; Xiong et al., 2020). Here, we selected one target at each end, 5′ and 3′, of the SARS-CoV-2 genome, aiming to detect infectious viral RNA rather than subgenomic RNA or partially degraded molecules (Kim et al., 2020) (Figure 2A, Table S1). Multiple alignment analysis of available viral genomes (as of March 2020) highlighted regions in the ORF1ab and N genes that were highly conserved (Table S1). In addition, the potential detection *loci* encountered were screened for structured RNA segments and CRISPR-Cas12a compatible sequences (Table S1). The conserved region II (CII) located within the ORF1ab gene complied with the above premises and was used in this study. In addition, a previously reported sequence was selected for the N gene (N) (Broughton et al., 2020). More recently, mutation profile analysis of SARS-CoV-2 genomes showed that both targeted regions display mutation frequency within the genome-wide baseline (Azgari et al., 2021; Kosuge et al., 2020). Furthermore, no non-synonymous mutations associated with the variants are present within the selected detection targets of this work (Koyama et al., n.d.; Peacock et al., 2021) (Table S1). For quality control of the clinical sample, we employed the human RNaseP gene (Figure S2) (Broughton et al., 2020).

RT-PCR optimization and primer selection

Most of molecular tools to detect SARS-CoV-2 use a combination of an RT and a DNA polymerase followed by result visualization using real-time thermocyclers, limiting LMICs. These countries could overcome such limitations with alternative readouts, i.e., from in-gel visualization or fluorescence-mediated direct observation under a transilluminator. Here, we describe the optimization of the reported conditions for M-MLV RT and Taq DNA polymerase as adapted from the open-source protocol BEAR-mix for RT-PCR (Graham et al., 2021). RT-PCRs can be done in a single-step or two-step workflow. First, we compared the amplification performance using both enzymes in a single reaction versus adding Taq DNA polymerase once the RT step was completed, as differences in efficiency have been reported (Paula et al., 2004; Wacker and Godard, 2005). We used CRISPR-Cas12a as a method for comparing the amplification results using the fluorescence ratio between the test sample and the non-template control. No considerable differences were observed for samples with high viral load, whereas a fluorescence ratio greater than 2 was observed in low viral load samples for the one-step approach (Figure S3). Then, we evaluated the duration of the reverse transcription reaction. A 2.3-fold increase in the signal ratio was observed for samples with low viral load at 20 min of reverse transcription compared with 10 min (Figure S3). Thus, a single-step RT-PCR using 20 min of retro-transcription was suitable.

Based on the previously selected conditions, we performed titrations for both enzymes. We found that final concentrations of 1.6 ng/μL of Taq DNA polymerase and 1.7 ng/μL of M-MLV RT were sufficient to achieve a fluorescence ratio ≥ 2 for both high and low viral RNA load samples (Figure S3). The viral RNA sample volume was evaluated to determine if the fluorescence signal in low viral load samples could be increased. However, no substantial differences were observed, and 2 μL of sample volume in a 20 μL final reaction volume was used for the following standardization protocol (Figure S3). Finally, five primer sets for each detection *locus* were evaluated under the optimized RT-PCR amplification using a CRISPR-Cas12a assay (Figures 2A; Table S1). Primer set 3 was selected for both detection *loci* (Figures 2B–2E). Amplification with the selected primers generated 168 and 131 bp PCR products for ORF1ab and N, respectively. Strong fluorescence in the CRISPR-Cas detection reaction was observed for the ORF1ab target with a mean of 18-fold fluorescence ratio at 30 min (Figures 2B and 2C). The fluorescence ratio for the N target was slightly lower than that for ORF1ab, likely due to an increased non-specific fluorescence signal for the non-template control (Figures 2D and 2E).

Optimization of the CRISPR-Cas12a detection system

Several factors can influence the fluorescence readout in CRISPR-Cas detection assays, such as the Cas:crRNA molar ratio, crRNA sequence, fluorophore quencher (FQ)-labeled ssDNA reporter probe, magnesium concentration, or reaction temperature (Bai et al., 2019; Huang et al., 2020; Tsou et al., 2019). We evaluated three variables for the system based on reported conditions (Broughton et al., 2020), for both SARS-CoV-2 targets and the human RNaseP control. First, a range between 5 and 50 nM LbCas12a was titrated against 15 nM crRNA. This showed that 10 nM Cas12a was sufficient for a fluorescence ratio >3 for N and ORF1ab targets. Similarly, a fluorescence ratio of 2.5 was the case for the control target RNaseP with 10 nM Cas12a (Figure 2F). As for the N target, higher Cas12a concentrations showed higher non-specific noise, with the consequent reduction of the fluorescence ratio. On the other hand, for ORF1ab, a higher concentration of Cas12a did not show a similar effect, the highest fluorescence ratio was found with 25 nM Cas12a at 30 min (Figure 2F). However, after 90 min of the reaction, an increasing non-specific signal was observed for Cas12a concentrations starting at 5 nM. For the RNaseP target, higher Cas12a concentration increased the fluorescence ratio (Figure 2F).

Next, we tested crRNA concentration at a range between 5 and 100 nM against 10 nM LbCas12a (Figure 2G). For all targets, 15 nM crRNA resulted in the highest fluorescence ratio, more than 2-fold at 30 min. For all targets, crRNA concentrations of more than 25 nM showed increased non-specific backgrounds (Figure 2G). Also, a range between 2.5 and 20 mM $MgCl_2$ was evaluated (Figure 2H). For the N target, no considerable differences in the fluorescence ratio were observed between 10 and 20 mM $MgCl_2$. On the other hand, for ORF1ab and RNaseP targets, the highest fluorescence ratios (>10) were observed with 15 mM $MgCl_2$ or higher at 30 min (Figure 2H). Finally, the selected optimal conditions for sample testing were 10 nM LbCas12a, 15 nM crRNA, and 15 mM $MgCl_2$. In addition, a synthetic dsDNA template for each target was used to estimate the analytical sensitivity of the selected conditions (Figure S4). A 10-fold serial dilution of each dsDNA template (10 nM to 1 pM) was evaluated, and a 1.5 fluorescence ratio was arbitrarily considered as a threshold value of detection. For the N target, 1 nM was the minimal concentration of molecules detected. In contrast, ORF1ab and RNaseP targets could be detected at 10 times lower concentration than N, allowing the detection of 100 pM (Figure S4).

Analytical sensitivity estimation

To assess the detection limit of the optimized CRISPR-based detection system coupled to RT-PCR, we used purified SARS-CoV-2 genomic RNA (isolate USA-WA1/2020, BEI Resources: NR-52347). For the ORF1ab target, high fluorescence ratios were observed for at least 5×10^2 ge/μL at 30 min. Lower viral RNA copy numbers resulted in a drastic decrease in the fluorescence signal as observed by the reduced fluorescence ratios toward 3-fold (Figures 3A and 3C). Likewise, detection of the N target was achieved up to 10^2 ge/μL, differentiating from the blank reaction with a fluorescence ratio >3.5 (Figures 3B and 3C). Considering a fluorescence ratio of at least 1.5, a limit of detection of 10^2 ge/μL was reported for both viral targets. Our locally produced enzymes for RT-PCR and optimized conditions were compared with a commercial one-step RT-PCR kit (Norgen BioTek) using the N primer set (Figure 3C). Fluorescence ratios from the commercial kit were similar to the ratios for the ORF1ab target and 2-fold higher than for the N target obtained with the produced enzymes (Figure 3C). This likely results from the 2-fold increase in the initial velocity (V_0) in the non-template control (RT-PCR blank) for the N target compared with the ORF1ab. Thus, no apparent differences were observed when V_0 of the fluorescence time courses was used (Figure 3D).

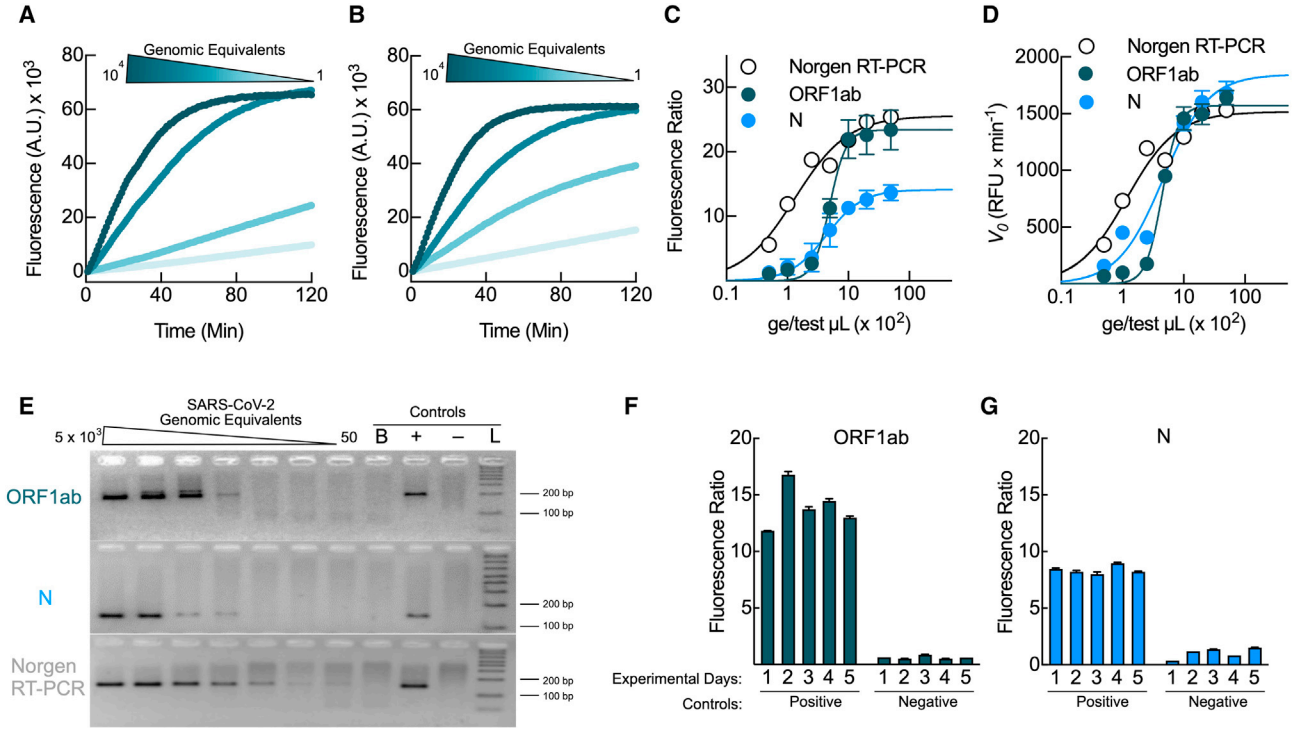

Figure 3. Analytical validation of SARS-CoV-2 RNA detection

(A) Time courses of the CRISPR-Cas12a-mediated detection of ORF1ab at increasing genome equivalents of SARS-CoV-2 RNA. Selected time traces are colored in shades of green for genome equivalents decreasing by a factor of 10 from 10^4 (dark green) to 10^2 (light green) per reaction in addition to the blank control (lightest).

(B) As in (A), for the N *locus*.

(C) Comparison of the fluorescence ratio as a function of input genome equivalents of SARS-CoV-2 RNA in the RT-PCR for ORF1ab and N *loci* and the commercial 2X One-Step RT-PCR Master Mix from Norgen.

(D) Initial velocity (V_0) dependency on genome equivalents.

(E) Gel electrophoresis analysis of RT-PCR products with varying genome equivalents for ORF1ab and N, and using the Norgen BioTek commercial one-step kit.

(F) and (G) show day-to-day reproducibility assays for ORF1ab and N *loci*, respectively. Error bars represent the standard deviation of at least three independent measurements.

An alternative to the fluorescence readout for LMICs is to use widely available gel electrophoresis. Gel visualization of the amplification products showed expected bands for ORF1ab (168 bp) and N (131 bp) targets up to 5×10^2 ge/µL in the RT-PCR. Unlike the commercial kit, visible bands were detected at 2.5×10^2 ge/µL, with weak bands up to 5×10^1 ge/µL (Figure 3E). Finally, the reproducibility of the CRISPR-Cas12a method was evaluated along five different days using sample pools for positive and negative controls. Very limited day-by-day variation was observed (Figures 3F and 3G). Average fluorescence ratios of 14 ± 2 and 0.6 ± 0.1 RFU were estimated for the positive and negative controls of the ORF1ab target, respectively. Likewise, fluorescence ratios of 8.4 ± 0.3 and 1.1 ± 0.4 RFU were calculated for the positive and negative controls of the N target, respectively.

Clinical validation

Clinical evaluation of molecular methods used for SARS-CoV-2 detection have shown sensitivities ranging between 50% and 90% and a specificity near 99% (Stites and Wilen, 2020; Vandenberg et al., 2021; Wang et al., 2020). The diagnostic performance of our molecular toolkit was evaluated by testing clinical samples. One hundred clinical samples collected during 2020 were analyzed by the gold standard qRT-PCR test. Positives (N = 50) and negatives (N = 50) for SARS-CoV-2 were randomized and analyzed with the molecular toolkit developed here. Since the optimization assays showed that the fluorescence ratio of positive samples increases over time, we evaluated different time points to find an optimal measuring time. Even though an increment of a non-specific signal was observed, the fluorescence ratios were not affected within the first 60 min. No significant differences in the test performance were observed for the N ($p = 0.685$) and the ORF1ab targets ($p = 0.584$). We selected a reading time of 30 min for the detection of both viral targets as a good compromise between assay performance and workaround time. Clinical samples showed varying fluorescence ratios, between 0.71 and 11.98 for the N gene, and 0.45 and 19.95 for the ORF1ab (Figures 4A and 4B). Using V_0 as the outcome variable, positive samples presented a V_0 between 226 ± 2 and 1,695 ± 12 RFU min^{-1} and between 40 ± 1 and 1,614 ± 13 RFU min^{-1}, for the N and ORF1ab *loci*, respectively (Figure S5). Negative clinical samples resulted in low fluorescence ratios and V_0 (Figures 4A, 4B, and S5). For all

Please cite this article in press as: Alcántara et al., Unlocking SARS-CoV-2 detection in low- and middle-income countries, Cell Reports Methods (2021), https://doi.org/10.1016/j.crmeth.2021.100093

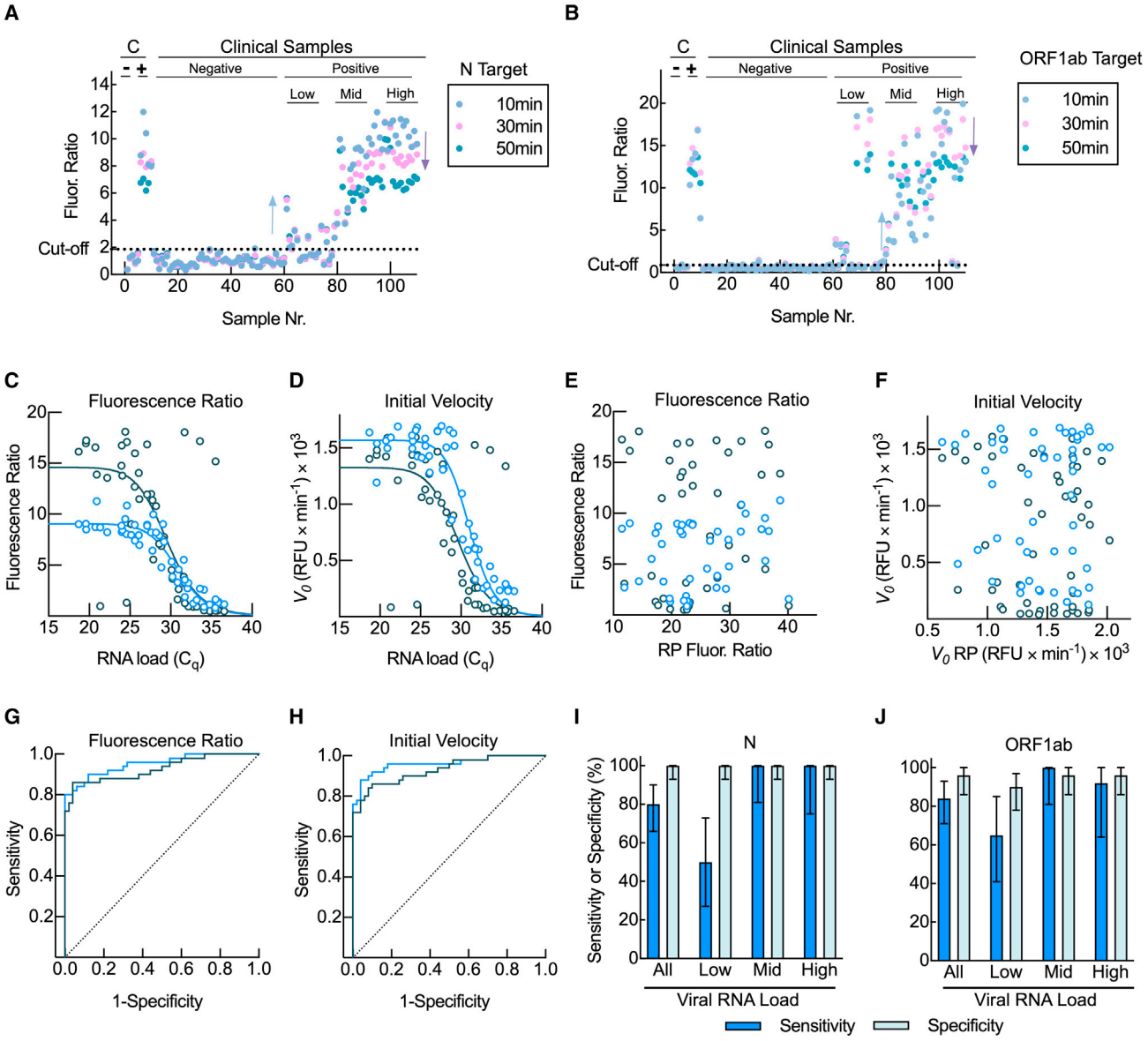

Figure 4. Test performance with clinical samples

(A) Distribution of fluorescence ratios for positive and negative controls (n = 10) and unknown samples (n = 100) for the N target. The dashed line indicates the threshold as calculated by the ROC analysis.

(B) As in (A), for the ORF1ab *locus*.

(C) Fluorescence ratio as a function of viral RNA load (Cq values) for both SARS-CoV-2 targets, N (blue) and ORF1ab (green).

(D–H) (D) Same as in (C), but using the initial velocity (V_0). Fluorescence ratio (E) and initial velocity (F) dependence for ORF1ab and N as a function of the sample control RNaseP target. Colors are as in (C). ROC curve based on fluorescence ratio (G) or initial velocity (H). ROC curves were obtained independently for each evaluated SARS-CoV-2 target; colors are as in (C).

(I) N target detection sensitivity and specificity with 95% CI (error bars) for all samples and by viral RNA load, namely high (Cq<25), medium (Cq=25–31), and low (Cq>31).

(J) As in (I), for the ORF1ab target.

positive samples, fluorescence ratios and V_0 were considerably higher than for the negative controls, while for the RNaseP sample control, both outcome readouts were broadly distributed (Figure S5). The fluorescence ratios and V_0 for both N and ORF1ab targets showed a positive dependence on the viral RNA load of the samples (Figures 4C and 4D), while no correlation was observed with the respective RNaseP fluorescence ratios or V_0 (Figures 4E and 4F). Thus, the performance of the molecular toolkit is dependent on the viral RNA load rather than on variations during sample collection or RNA extraction.

The detection boundaries were estimated by calculating a receiver operating characteristic (ROC) curve from the

fluorescence ratio and V_0 for both N and ORF1ab regions (Figures 4G and 4H). No significant difference was observed between the ROC curves by either analytical approach ($p = 0.508$). The sensitivity and specificity using the fluorescence ratio and V_0 data analysis were determined for all samples and within groups based on viral RNA load (Figures 4I and 4J; Tables S2 and S3). For the N target, the overall sensitivity and specificity, as calculated using fluorescence ratios and a cutoff of 1.86, were 80% and 100%, respectively. If V_0 was used, the analysis showed 88% sensitivity and 96% specificity (cutoff value of 253 RFU min^{-1}) (Figure 4I; Table S2). The samples that were misclassified by the fluorescence ratio threshold showed a Cq value >33 and $V_0 < 300$ RFU min^{-1}. However, two of the correctly classified samples presented Cq values of 34 but $V_0 > 330$ RFU min^{-1}. On the other hand, for the ORF1ab target, the fluorescence ratio analysis (cutoff value of 0.86) showed 84% sensitivity and 96% specificity, whereas the V_0 analysis (cutoff value of 73 RFU min^{-1}) showed a sensitivity of 86% and a specificity of 90% (Figure 4J; Table S2). Similarly, as to N target detection, false negative results presented a Cq value >33 but with $V_0 < 450$ RFU min^{-1}. Nonetheless, five true positive results showed a Cq > 33 with V_0 ranging between 226 and 277 RFU min^{-1}. With regard to the false positive results reported herein, a $V_0 <$ 360 RFU min^{-1} was estimated (Cq values were not determined as they were negative with the gold standard). Visual detection by gel electrophoresis showed lower sensitivity values for both N (66%) and ORF1ab (50%) targets, but similar specificity to fluorescence readout (Table S2). All samples were categorized by RNA load using the Cq values, namely high (<25), medium (25–31), and low (>31). Our results show an increased sensitivity for both targets in samples with medium to high viral RNA loads, achieving 100% sensitivity. The increase was independent of the analysis used, either fluorescence ratios or V_0 analysis (Table S3). However, samples with low viral RNA load showed lower sensitivity, less than 70% (Figures 4I and 4J; Table S3).

Unlocking remote locations with Bento Lab

The demand for molecular testing can exponentially escalate as the pandemic expands to poorly accessible areas. For instance, Peru, a country characterized by social and economic disparities if comparing cities with small towns, holds the highest death toll per million habitants. Its small towns still lack accessibility to molecular testing, even more than a year into the COVID-19 pandemic. There are several reasons that can account for such shortages in LMICs, a prominent one being the lack of any laboratory infrastructure in remote rural cities, towns, and communities. To cope with these limitations, we applied the molecular toolkit established here using the portable laboratory from Bento Lab that consists of a thermocycler for 32 samples, a microcentrifuge, a gel electrophoresis chamber, and a small transilluminator (Figure 5A). We show that the Bento Lab is capable of amplifying SARS-CoV-2 genetic material (Figure 5B) and allows the visualization of results with our molecular toolkit (Figures 5B and 5C). Furthermore, a comparison of the amplification of target RNA between the Bento Lab and a regular thermocycler by quantitatively measuring Cas12a-dependent fluorescence shows that the portable laboratory can be a solid alternative (Figure 5). Thus, the molecular toolkit described here can potentially unlock the molecular detection of pathogenic agents even in resource-limited regions.

DISCUSSION

A prompt epidemiological surveillance of infectious diseases requires decentralized detection capacity, acquired by enabling direct detection of the pathogenic entity in primary health care and available laboratories. Although many alternative methods have been described, RT-PCR remains the gold standard for detection of SARS-CoV-2 and other respiratory viruses (Beck and Henrickson, 2010; Benzigar et al., 2020; Böger et al., 2021; Lin et al., 2020). Furthermore, PCR and qPCR methods are a straightforward analytical solution for a number of emerging pathogens. For instance, they were rapidly deployed in recent virus outbreaks, including influenza, SARS and MERS, Zika, dengue, and chikungunya, among others, that pose a serious threat to humans, either because of their pandemic potential or due to their recurrent appearance affecting communities in LMICs severely (Johani and Hajeer, 2016; Johnson et al., 2016; Ravina et al., 2021; Silva et al., 2019). Scientists and health professionals promptly developed solutions to cope with the lack of molecular detection platforms. Thus, LMICs have the theoretical and practical bases to rapidly design, validate, and use PCR-based methods for any pathogenic threat. Yet, the COVID-19 pandemic unmasked an unexpected complication: a shortage of laboratory testing supplies due to an unprecedented global demand. Paradoxically, globalization hampered LMICs' access to molecular detection solutions, yet unlocked the access to information for driving local efforts to deal with the global market limitations. The latter is further evidenced by several remarkable open-access initiatives, like BEARmix (Graham et al., 2021), Addgene (https://www.addgene.org/), BEI Resources (https://www.beiresources.org/), Nextstrain (https://nextstrain.org/), and GISAID (https://www.gisaid.org/). The work presented here was fully performed in an LMIC laboratory and used all available open-access resources to implement a molecular toolkit aiming to provide versatile solutions for LMICs and to cope with the international shortage of testing supplies for SARS-CoV-2 or any other pathogenic agent.

The molecular toolkit validated here shows high versatility for adaptation to different contexts by exploiting widely accepted and known PCR-based methods (Figure 5A). The initial stage focused on providing a minimal set of essential recombinant enzymes that allows the amplification and visualization of viral genes in laboratories with minimal equipment. The open-access BEARmix initiative was particularly important, as they kindly provided plasmids, protocols, and initial conditions alongside their development and prior to any publication (Graham et al., 2021). Yet, some routines of the protein production workflow needed to be adapted due to equipment availability. For instance, enzyme production can be achieved to high purity in laboratories lacking an FPLC instrument by using salt gradients set up manually and inexpensive plastic syringes. This, in turn, allows any laboratory with minimal *E. coli* cultivation capacities to produce high-purity enzymes. Other simpler methods have also been reported and could be tested. Bhadra et al. used crude heat-treated extracts as a source of Taq, Phusion, and Bst DNA polymerases and M-MLV RT enzymes, with promising results

Please cite this article in press as: Alcántara et al., Unlocking SARS-CoV-2 detection in low- and middle-income countries, Cell Reports Methods (2021), https://doi.org/10.1016/j.crmeth.2021.100093

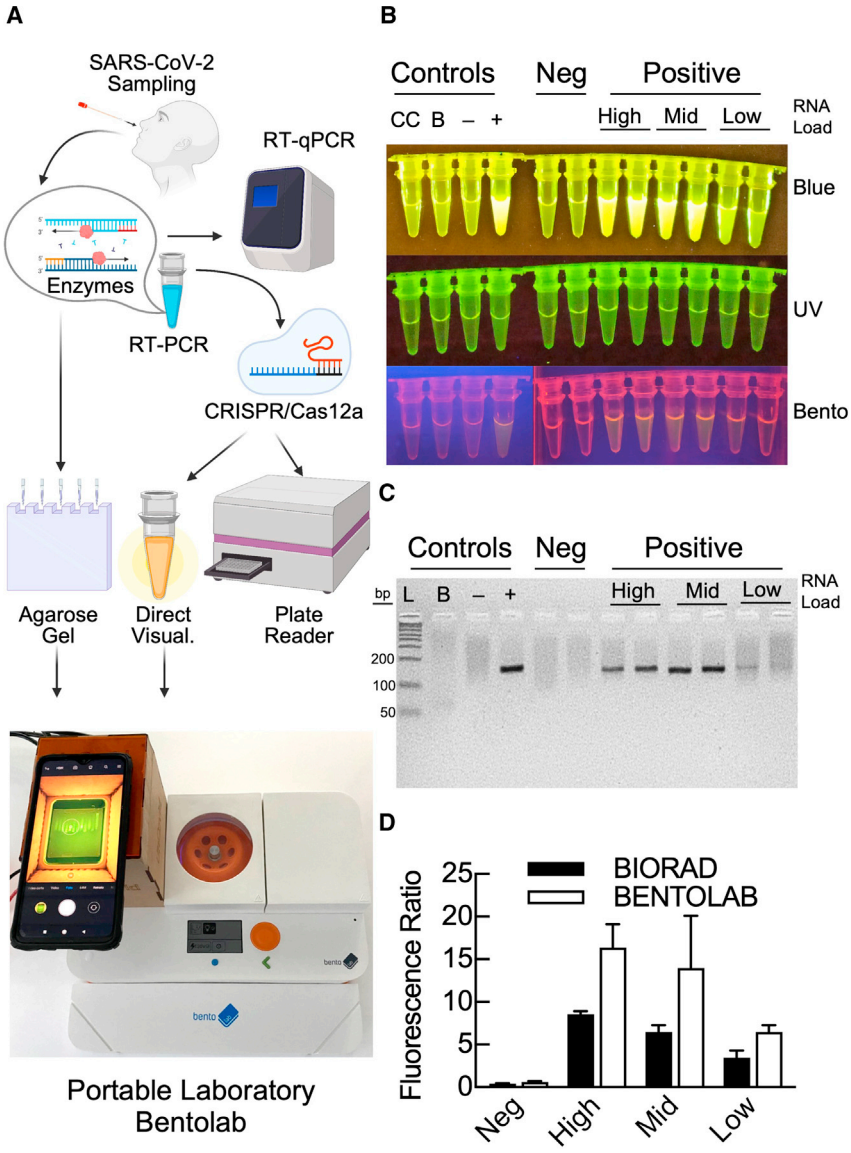

Figure 5. Alternative readouts and portability of molecular detection with Bento Lab.

(A) Scheme of the different analytical options for the method reported here.

(B–D) Two clinical samples of each viral RNA load group (low, medium, and high) and two negative samples were analyzed using the N target. (B) Fluorescent signals visualized in tubes using three different transilluminators: blue light (470 nm) (top), UV (middle), and Bento Lab (bottom). Controls included the CRISPR control (i.e., Cas12a reaction without amplified target DNA) for assessing background fluorescence (CC), the RT-PCR non-template control (blank, B), and pools of negative (–) or positive (+) samples. (C) Agarose gel (5%) electrophoresis of conventional RT-PCR-amplified products. L, DNA ladder; B, a PCR blank reaction (no template); plus and minus signs indicate positive and negative controls, respectively. (D) Ratio of CRISPR-Cas12a fluorescent signals of the test sample relative to the RT-PCR non-template control. Error bars indicate standard errors obtained from duplicate experiments.

(Bhadra et al., 2018). In addition to RT-PCR enzymes, we report the production of LbCas12a, also in a minimal laboratory setup. Altogether, the proposed 4-day/person workflow allows the production of enzymes for over 50,000 tests. Further scaling or implementation in multiple laboratories could satisfy the testing needs of an entire city or country. Each detection reaction costs approximately $1.02, which means that a panel of 90 samples plus positive and negative controls could cost around $100. The costs for locally implementing the method may vary depending on available equipment. The funding for the development and validation of the molecular toolkit described here amounted to $100,000, covering the acquisition of several pieces of equipment, pipettes, materials, and salaries for four junior researchers. If some equipment is already available, these costs can be drastically reduced.

The focus on RT-PCR methods unlocks several alternatives for visualizing the presence or absence of a target genetic material in a patient sample (Figure 5A). Such versatility is further enhanced by coupling RT-PCR to detection mediated by CRISPR-Cas12a. In this context, the production of crRNA molecules from DNA templates can be easily performed to satisfy the demand (Figure S1). In addition, CRISPR-Cas12a can be used in both qualitative and quantitative detection ways. The direct visualization of fluorescence in tubes allows any laboratory using a blue-light transilluminator to qualitatively assign the presence or absence of amplified genetic material (Figure 5B) (Chen et al., 2020; Ding et al., 2020; Huang et al., 2020; Pang et al., 2020; Xiong et al., 2020). Our system is capable of detecting an observable signal after only 15 min of the CRISPR-Cas12a reaction (Figure S6). Another low-cost method uses widely available gel electrophoresis systems. Although the sensitivity is lower than that of fluorescence-based methods (Figure S7; Table S3), agarose gel electrophoresis offers an alternative for laboratories equipped with only a thermocycler and transilluminator. Importantly, the specificity by agarose gel electrophoresis is not compromised and the sensitivity for high viral RNA load samples is still competitive (Figure S7). Although not tested here, Graham et al. used TaqMan probes for direct visualization of genetic material using transilluminators with high sensitivity (Graham et al., 2021). Thus, also in the absence of LbCas12a, the molecular toolkit could be coupled to direct visualization of test results in laboratories with minimal molecular biology facilities.

Fluorescence plate readers are common in different laboratory setups and could be used for quantitative detection of SARS-CoV-2 (Figures 3 and 4) (Ding et al., 2020; Ganguli et al., 2020; Sun et al., 2021; Woo et al., 2020;

Xiong et al., 2020). Our toolkit used clinical samples to determine critical detection parameters, showing competitive sensitivity and specificity (Figure 4). Although the specificity was high regardless of viral RNA load, the sensitivity decreased with lower viral RNA load (Figures 4I and 4J). Thus, low viral loads may result in false negative results. Yet, molecular detection is one variable that is considered to assess the likelihood of infection that a person may hold. Indeed, most diagnostic algorithms also consider symptoms, comorbidities, vicinity to diagnosed contacts, and prevalence of SARS-CoV-2 in the population being tested, among other factors. Thus, even low sensitivity in detection systems can greatly contribute to better diagnostic assessments at the clinical level. Our system shows an overall sensitivity of 86% for samples of unknown viral load, and this increases to 100% for patients with medium to high viral load. A recent study found that Cq values greatly varied among SARS-CoV-2-infected people, with a distribution peaking at Cq values of 23–25 (Buchan et al., 2020). In that context, our system should be able to correctly detect all analyzed samples.

Altogether, the presented study reports a molecular toolkit that can be produced and used in a variety of laboratory setups. Furthermore, the Bento Lab portable laboratory could unlock molecular detection even in low-resource settings lacking any laboratory infrastructure. Poor infrastructure combined with reduced accessibility to reagents could be overcome in LMICs. This work reports on a molecular detection platform entirely produced in an LMIC laboratory setup, providing detailed methods and final protocols to be used, which can be adapted for any forthcoming pathogenic threat.

Limitations of study

Laboratory-developed tests (LDTs), considered as *in vitro* diagnostics (IVD) and intended for clinical use, can be designed, manufactured, and used within a single laboratory (Genzen, 2019). Regulations for LDTs are covered by the Food and Drug Administration (FDA) in the United States or the HIC counterparts with a clear framework (US Food and Drug Administration, 2014). In contrast, many LMICs lack these regulations, prompting their institutions to import and validate tests. In a sense, imported platforms do have a regulatory framework for clinical use while local production is not covered in LMICs. A missing framework for regulating LDTs appeared as a bottleneck in LMICs and needed to be newly developed using HICs as a starting point; yet, scarce resource settings may not be fully considered (Piaggio et al., 2021). This legal and infrastructural void is fed by the lack of laboratories developing LDTs, maintaining a dependence on imports and availability on the global market. Upscaling the production industrially brings up a different level of complexity in both infrastructural and regulatory policies. The availability of good manufacturing practices (GMP)-certified plants is very limited in LMICs. Similar to LDTs, policies for mass production of IVDs are poorly represented across LMICs. Emergency amendments have been issued all over the world due to COVID-19 as a rapid alternative to unlock the above limitations. The US Department of Health and Human Services (HHS) has overruled the FDA premarket review process of approval for LDTs in certain cases for SARS-CoV-2 detection, opening a gray zone of regulations even in the United States, a country with a well-established framework (US Food and Drug Administration, 2021). Laboratory certifications to perform diagnostics are more widely regulated in LMICs. As specified by the Clinical Laboratory Improvement Amendments (CLIA), non-certified laboratories are allowed to perform SARS-CoV-2 screenings with molecular technology, provided that the samples are non-patient specific, i.e., using pooled samples (U.S. Centers for Medicare & Medicaid Services, 2020). A laboratory willing to use pooling with a SARS-CoV-2 nucleic-acid-based test would be expected to evaluate and validate the test performance for a pooling strategy (National Center for Immunization and Respiratory Diseases [NCIRD], Division of Viral Diseases, 2021). Pooling samples is encouraged by the FDA and recommended as a long-term strategy to monitor COVID-19 in LMICs (Chowdhury et al., 2020). The method reported here accounts as an opportunity for LMICs to use LDTs to compensate for unavailability of molecular testing. However, the implementation remains limited by the availability of local regulatory policies, which vary widely from country to country. The implementation and usage of the method reported here or any other method must address local regulatory frameworks.

Developing, validating, and implementing LDTs imply technical procedures that must be taken into consideration to ensure reliable results. Laboratories implementing the reported molecular detection methods should adhere to specific protocols to avoid amplicon contamination, which can increase the number of false positives. This limitation is a well-known issue reported in clinical laboratories (Aslanzadeh, 2004) and for SARS-CoV-2 detection (Davidi et al., 2021). As found previously, research laboratories are especially prone to finding amplicon traces on high-frequency-contact surfaces and personal objects (Davidi et al., 2021). Adherence to a cleaning protocol for doorknobs, lab notebooks, pens, glasses, computer keyboards, etc., is important to prevent and mitigate this risk. Trained personnel are essential for the correct use of equipment, pipetting technique, usage of filter tips, and area-specific glove replacement (WHO's Dos and Don'ts for molecular testing, 2021). Particularly, handling of all post-amplification steps (i.e., electrophoresis, CRISPR-Cas12a-mediated detection, or other) must be restrained to a dedicated laboratory space. Most clinical laboratory certifications require procedures that implement a unidirectional flow of samples considering "clean" and "dirty" laboratory areas to avoid amplicon contamination. Opening post-amplification tubes should be avoided whenever possible and restricted to a single laboratory space. Alternatively, dUTP can be used in all nucleic-acid amplification steps to generate deoxyuridine-containing amplicons, which can be removed from further reactions by adding uracil N-glycosylase (Pennings et al., 2001). Although we did not test it, the usage of dUTP was shown to be compatible with CRISPR-Cas12a-based detection methods (Qian et al., 2019). Finally, sample handling and good clinical laboratory practices (GCLP) are essential (see Dos and Don'ts for molecular testing, World Health Organization, 2021), and online training in GCLP is recommended and necessary (https://www.cdc.gov/labtraining/training-courses/good-lab-practices-molecular-genetics-testing.html).

STAR★METHODS

Detailed methods are provided in the online version of this paper and include the following:

- KEY RESOURCES TABLE
- RESOURCE AVAILABILITY
  - Lead contact
  - Materials availability
  - Data and code availability
- EXPERIMENTAL MODEL AND SUBJECT DETAILS
  - Microbes
  - Nasopharyngeal swabs collection
- METHOD DETAILS
  - Protein expression and purification
  - crRNAs preparation
  - RT-PCR assays
  - CRISPR-Cas12a *trans*-cleavage assays
  - End-point CRISPR-Cas12a assays
  - Clinical samples and validation
  - Bioinformatic analyses
- QUANTIFICATION AND STATISTICAL ANALYSIS

SUPPLEMENTAL INFORMATION

Supplemental information can be found online at https://doi.org/10.1016/j.crmeth.2021.100093.

ACKNOWLEDGMENTS

We are very thankful to Dr. Marcos Milla for donating equipment that was used in this study. We would also like to thank all lab members of the del Valle, Adaui, and Milón groups for their help, support, helpful discussions, and great working atmosphere. This work was supported by grants from the peruvian Fondo Nacional de Desarrollo Científico Tecnológico y de Innovación Tecnológica [070-2020-FONDECYT] to V.A. and [036-2019-FONDECYT-BM-INC.INV] to P.M.

AUTHOR CONTRIBUTIONS

Conceptualization and methodology, R.A., K.P., V.A., and P.M.; investigation, R.A., K.P., J.A.N., G.M.R., and J.M.L.; formal analysis, R.A., K.P., J.A.N., J.D.V.M., and P.M.; writing – original draft, R.A., K.P., J.A.N., and P.M.; writing – review & editing, R.A., K.P., J.A.N., G.M.R., V.A., J.D.V.M., and P.M.; visualization, K.P., J.A.N., R.A., and P.M.; supervision, J.D.V.M., V.A., and P.M.; project administration, P.M.

DECLARATION OF INTERESTS

The authors declare no competing interests.

Received: April 9, 2021
Revised: July 31, 2021
Accepted: September 20, 2021
Published: October 25, 2021

REFERENCES

Abbott, S., Hellewell, J., Thompson, R.N., Sherratt, K., Gibbs, H.P., Bosse, N.I., Munday, J.D., Meakin, S., Doughty, E.L., Chun, J.Y., et al. (2020). Estimating the time-varying reproduction number of SARS-CoV-2 using national and subnational case counts. Wellcome Open Res. *5*, 112.

Adepoju, P. (2020). Africa's struggle with inadequate COVID-19 testing. Lancet Microbe *1*, e12.

Alekseenko, A., Barrett, D., Pareja-Sanchez, Y., Howard, R.J., Strandback, E., Ampah-Korsah, H., Rovšnik, U., Zuniga-Veliz, S., Klenov, A., Malloo, J., et al. (2021). Direct detection of SARS-CoV-2 using non-commercial RT-LAMP reagents on heat-inactivated samples. Sci. Rep. UK *11*, 1820.

Ali, Z., Aman, R., Mahas, A., Rao, G.S., Tehseen, M., Marsic, T., Salunke, R., Subudhi, A.K., Hala, S.M., Hamdan, S.M., et al. (2020). iSCAN: an RT-LAMP-coupled CRISPR-Cas12 module for rapid, sensitive detection of SARS-CoV-2. Virus Res. *288*, 198129.

Aslanzadeh, J. (2004). Preventing PCR amplification carryover contamination in a clinical laboratory. Ann. Clin. Lab. Sci. *34*, 389–396.

Azgari, C., Kilinc, Z., Turhan, B., Circi, D., and Adebali, O. (2021). The mutation profile of SARS-CoV-2 is primarily shaped by the host antiviral defense. Viruses *13*, 394.

Bai, J., Lin, H., Li, H., Zhou, Y., Liu, J., Zhong, G., Wu, L., Jiang, W., Du, H., Yang, J., et al. (2019). Cas12a-Based on-site and rapid nucleic acid detection of african swine fever. Front. Microbiol. *10*, 2830.

Beck, E.T., and Henrickson, K.J. (2010). Molecular diagnosis of respiratory viruses. Future Microbiol. *5*, 901–916.

Benzigar, M.R., Bhattacharjee, R., Baharfar, M., and Liu, G. (2020). Current methods for diagnosis of human coronaviruses: pros and cons. Anal. Bioanal. Chem., 1–20.

Bhadra, S., Pothukuchy, A., Shroff, R., Cole, A.W., Byrom, M., Ellefson, J.W., Gollihar, J.D., and Ellington, A.D. (2018). Cellular reagents for diagnostics and synthetic biology. PLoS One *13*, e0201681.

Bhadra, S., Riedel, T.E., Lakhotia, S., Tran, N.D., and Ellington, A.D. (2020). High-surety isothermal amplification and detection of SARS-CoV-2, including with crude enzymes. Biorxiv.

Böger, B., Fachi, M.M., Vilhena, R.O., Cobre, A.F., Tonin, F.S., and Pontarolo, R. (2021). Systematic review with meta-analysis of the accuracy of diagnostic tests for COVID-19. Am. J. Infect. Control *49*, 21–29.

Broughton, J.P., Deng, X., Yu, G., Fasching, C.L., Servellita, V., Singh, J., Miao, X., Streithorst, J.A., Granados, A., Sotomayor-Gonzalez, A., et al. (2020). CRISPR–Cas12-based detection of SARS-CoV-2. Nat. Biotechnol. *38*, 870–874.

Buchan, B.W., Hoff, J.S., Gmehlin, C.G., Perez, A., Faron, M.L., Munoz-Price, L.S., and Ledeboer, N.A. (2020). Distribution of SARS-CoV-2 PCR cycle threshold values provide practical insight into overall and target-specific sensitivity among symptomatic patients. Am. J. Clin. Pathol. *154*, aqaa133.

Chen, J.S., and Doudna, J.A. (2017). The chemistry of Cas9 and its CRISPR colleagues. Nat. Rev. Chem. *1*, 0078.

Chen, J.S., Ma, E., Harrington, L.B., Costa, M.D., Tian, X., Palefsky, J.M., and Doudna, J.A. (2018). CRISPR-Cas12a target binding unleashes indiscriminate single-stranded DNase activity. Science *360*, eaar6245.

Chen, Y., Shi, Y., Chen, Y., Yang, Z., Wu, H., Zhou, Z., Li, J., Ping, J., He, L., Shen, H., et al. (2020). Contamination-free visual detection of SARS-CoV-2 with CRISPR/Cas12a: a promising method in the point-of-care detection. Biosens. Bioelectron. *169*, 112642.

Chowdhury, R., Heng, K., Shawon, M.S.R., Goh, G., Okonofua, D., Ochoa-Rosales, C., Gonzalez-Jaramillo, V., Bhuiya, A., Reidpath, D., Prathapan, S., et al. (2020). Dynamic interventions to control COVID-19 pandemic: a multivariate prediction modelling study comparing 16 worldwide countries. Eur. J. Epidemiol. *35*, 389–399.

Corman, V.M., Landt, O., Kaiser, M., Molenkamp, R., Meijer, A., Chu, D.K., Bleicker, T., Brünink, S., Schneider, J., Schmidt, M.L., et al. (2020). Detection of 2019 novel coronavirus (2019-nCoV) by real-time RT-PCR. Eurosurveillance *25*, 2000045.

Davidi, D., Fitzgerald, S., Glaspell, H.L., Jalbert, S., Klapperich, C.M., Landaverde, L., Maheras, S., Mattoon, S.E., Britto, V.M., Nguyen, G.T., et al. (2021). Amplicon residues in research laboratories masquerade as COVID-19 in surveillance tests. Cell Rep. Methods *1*, 100005.

Ding, X., Yin, K., Li, Z., Lalla, R.V., Ballesteros, E., Sfeir, M.M., and Liu, C. (2020). Ultrasensitive and visual detection of SARS-CoV-2 using all-in-one dual CRISPR-Cas12a assay. Nat. Commun. *11*, 4711.

Esbin, M.N., Whitney, O.N., Chong, S., Maurer, A., Darzacq, X., and Tjian, R. (2020). Overcoming the bottleneck to widespread testing: a rapid review of nucleic acid testing approaches for COVID-19 detection. RNA *26*, 771–783.

Ferretti, L., Wymant, C., Kendall, M., Zhao, L., Nurtay, A., Abeler-Dörner, L., Parker, M., Bonsall, D., and Fraser, C. (2020). Quantifying SARS-CoV-2 transmission suggests epidemic control with digital contact tracing. Science *368*, eabb6936.

Fozouni, P., Son, S., Derby, M.D.de L., Knott, G.J., Gray, C.N., D'Ambrosio, M.V., Zhao, C., Switz, N.A., Kumar, G.R., Stephens, S.I., et al. (2021). Amplification-free detection of SARS-CoV-2 with CRISPR-Cas13a and mobile phone microscopy. Cell *184*, 323–333.e9.

Ganguli, A., Mostafa, A., Berger, J., Aydin, M.Y., Sun, F., Ramirez, S.A.S.de, Valera, E., Cunningham, B.T., King, W.P., and Bashir, R. (2020). Rapid isothermal amplification and portable detection system for SARS-CoV-2. Proc. Natl. Acad. Sci. U S A *117*, 22727–22735.

Genzen, J.R. (2019). Regulation of laboratory-developed TestsA clinical laboratory perspective. Am. J. Clin. Pathol. *152*, 122–131.

Gootenberg, J.S., Abudayyeh, O.O., Lee, J.W., Essletzbichler, P., Dy, A.J., Joung, J., Verdine, V., Donghia, N., Daringer, N.M., Freije, C.A., et al. (2017). Nucleic acid detection with CRISPR-Cas13a/C2c2. Science *356*, 438–442.

Graham, T.G.W., Dugast-Darzacq, C., Dailey, G.M., Nguyenla, X.H., Dis, E.V., Esbin, M.N., Abidi, A., Stanley, S.A., Darzacq, X., and Tjian, R. (2021). Open-source RNA extraction and RT-qPCR methods for SARS-CoV-2 detection. PLoS One *16*, e0246647.

Hanley, J.A., and McNeil, B.J. (1982). The meaning and use of the area under a receiver operating characteristic (ROC) curve. Radiology *143*, 29–36.

Harrington, L.B., Burstein, D., Chen, J.S., Paez-Espino, D., Ma, E., Witte, I.P., Cofsky, J.C., Kyrpides, N.C., Banfield, J.F., and Doudna, J.A. (2018). Programmed DNA destruction by miniature CRISPR-Cas14 enzymes. Science *362*, eaav4294.

Hasell, J., Mathieu, E., Beltekian, D., Macdonald, B., Giattino, C., Ortiz-Ospina, E., Roser, M., and Ritchie, H. (2020). A cross-country database of COVID-19 testing. Sci. Data *7*, 345.

Hou, T., Zeng, W., Yang, M., Chen, W., Ren, L., Ai, J., Wu, J., Liao, Y., Gou, X., Li, Y., et al. (2020). Development and evaluation of a rapid CRISPR-based diagnostic for COVID-19. PLoS Pathog. *16*, e1008705.

Hu, X., Deng, Q., Li, J., Chen, J., Wang, Z., Zhang, X., Fang, Z., Li, H., Zhao, Y., Yu, P., et al. (2020). Development and clinical application of a rapid and sensitive Loop-mediated isothermal amplification test for SARS-CoV-2 infection. Msphere *5*, e00808–e00820.

Huang, M., Zhou, X., Wang, H., and Xing, D. (2018). Clustered regularly interspaced short palindromic repeats/cas9 triggered isothermal amplification for site-specific nucleic acid detection. Anal. Chem. *90*, 2193–2200.

Huang, Z., Tian, D., Liu, Y., Lin, Z., Lyon, C.J., Lai, W., Fusco, D., Drouin, A., Yin, X., Hu, T., et al. (2020). Ultra-sensitive and high-throughput CRISPR-powered COVID-19 diagnosis. Biosens. Bioelectron. *164*, 112316.

Ibn-Mohammed, T., Mustapha, K.B., Godsell, J., Adamu, Z., Babatunde, K.A., Akintade, D.D., Acquaye, A., Fujii, H., Ndiaye, M.M., Yamoah, F.A., et al. (2021). A critical review of the impacts of COVID-19 on the global economy and ecosystems and opportunities for circular economy strategies. Resour. Conserv. Recycl. *164*, 105169.

Javalkote, V.S., Kancharla, N., Bhadra, B., Shukla, M., Soni, B., Sapre, A., Goodin, M., Bandyopadhyay, A., and Dasgupta, S. (2020). CRISPR-based assays for rapid detection of SARS-CoV-2. Methods. https://doi.org/10.1016/j.ymeth.2020.10.003.

Jinek, M., Chylinski, K., Fonfara, I., Hauer, M., Doudna, J.A., and Charpentier, E. (2012). A programmable dual-RNA–Guided DNA endonuclease in adaptive bacterial Immunity. Science *337*, 816–821.

Johani, S.A., and Hajeer, A.H. (2016). MERS-CoV diagnosis: an update. J. Infect. Public Heal *9*, 216–219.

Johnson, B.W., Russell, B.J., and Goodman, C.H. (2016). Laboratory diagnosis of Chikungunya virus infections and commercial sources for diagnostic assays. J. Infect. Dis. *214*, S471–S474.

Joung, J., Ladha, A., Saito, M., Segel, M., Bruneau, R., Huang, M.W., Kim, N.-G., Yu, X., Li, J., Walker, B.D., et al. (2020). Point-of-care testing for COVID-19 using SHERLOCK diagnostics. medRxiv. https://doi.org/10.1101/2020.05.04.20091231.

Kapust, R.B., Tözsér, J., Fox, J.D., Anderson, D.E., Cherry, S., Copeland, T.D., and Waugh, D.S. (2001). Tobacco etch virus protease: mechanism of autolysis and rational design of stable mutants with wild-type catalytic proficiency. Protein Eng. Des. Sel *14*, 993–1000.

Kellner, M.J., Ross, J.J., Schnabl, J., Dekens, M.P.S., Heinen, R., Grishkovskaya, I., Bauer, B., Stadlmann, J., Menéndez-Arias, L., Fritsche-Polanz, R., et al. (2020). A rapid, highly sensitive and open-access SARS-CoV-2 detection assay for laboratory and home testing. bioRxiv. https://doi.org/10.1101/2020.06.23.166397.

Kevadiya, B.D., Machhi, J., Herskovitz, J., Oleynikov, M.D., Blomberg, W.R., Bajwa, N., Soni, D., Das, S., Hasan, M., Patel, M., et al. (2021). Diagnostics for SARS-CoV-2 infections. Nat. Mater. *20*, 593–605.

Kim, D., Lee, J.-Y., Yang, J.-S., Kim, J.W., Kim, V.N., and Chang, H. (2020). The architecture of SARS-CoV-2 transcriptome. Cell *181*, 914–921.e10.

Kosuge, M., Furusawa-Nishii, E., Ito, K., Saito, Y., and Ogasawara, K. (2020). Point mutation bias in SARS-CoV-2 variants results in increased ability to stimulate inflammatory responses. Sci. Rep. UK *10*, 17766.

n.d. Koyama, T., Platt, D., and Parida, L. n.d. Variant analysis of SARS-CoV-2 genomes. B World Health Organ 98, 495–504.

Kucharski, A.J., Klepac, P., Conlan, A.J.K., Kissler, S.M., Tang, M.L., Fry, H., Gog, J.R., Edmunds, W.J., group, C.C.-19 working; and Emery, J.C., et al. (2020). Effectiveness of isolation, testing, contact tracing, and physical distancing on reducing transmission of SARS-CoV-2 in different settings: a mathematical modelling study. Lancet Infect. Dis. *20*, 1151–1160.

Larkin, M.A., Blackshields, G., Brown, N.P., Chenna, R., McGettigan, P.A., McWilliam, H., Valentin, F., Wallace, I.M., Wilm, A., Lopez, R., et al. (2007). Clustal W and clustal X version 2.0. Bioinformatics *23*, 2947–2948.

Larsson, A. (2014). AliView: a fast and lightweight alignment viewer and editor for large datasets. Bioinformatics *30*, 3276–3278.

Li, L., Li, S., Wu, N., Wu, J., Wang, G., Zhao, G., and Wang, J. (2019). HOLMESv2: a CRISPR-Cas12b-assisted platform for nucleic acid detection and DNA methylation quantitation. Acs Synth. Biol. *8*, 2228–2237.

Lin, C.-Y., Hwang, D., Chiu, N.-C., Weng, L.-C., Liu, H.-F., Mu, J.-J., Liu, C.-P., and Chi, H. (2020). Increased detection of viruses in children with respiratory tract infection using PCR. Int. J. Environ. Res. Public Health *17*, 564.

Matute, T., Nuñez, I., Rivera, M., Reyes, J., Blázquez-Sánchez, P., Arce, A., Brown, A.J., Gandini, C., Molloy, J., Ramirez-Sarmiento, C.A., et al. (2021). Homebrew reagents for low cost RT-LAMP. medRxiv. https://doi.org/10.1101/2021.05.08.21256891.

Metsky, H.C., Freije, C.A., Kosoko-Thoroddsen, T.-S.F., Sabeti, P.C., and Myhrvold, C. (2020). CRISPR-based surveillance for COVID-19 using genomically-comprehensive machine learning design. bioRxiv. https://doi.org/10.1101/2020.02.26.967026.

National Center for Immunization and Respiratory Diseases (NCIRD), Division of Viral Diseases (2021). Interim Guidance for Use of Pooling Procedures in SARS-CoV-2 Diagnostic and Screening Testing (Center for Disease Control and Prevention (CDC)).

Pang, B., Xu, J., Liu, Y., Peng, H., Feng, W., Cao, Y., Wu, J., Xiao, H., Pabbaraju, K., Tipples, G., et al. (2020). Isothermal amplification and ambient visualization in a single tube for the detection of SARS-CoV-2 using loop-mediated amplification and CRISPR technology. Anal. Chem. *92*, 16204–16212.

Pardee, K., Green, A.A., Takahashi, M.K., Braff, D., Lambert, G., Lee, J.W., Ferrante, T., Ma, D., Donghia, N., Fan, M., et al. (2016). Rapid, low-cost detection of Zika virus using programmable biomolecular components. Cell *165*, 1255–1266.

Paula, S.O.D., Lima, C.de M., Torres, M.P., Pereira, M.R.G., and Fonseca, B.A.L.da (2004). One-Step RT-PCR protocols improve the rate of dengue diagnosis compared to Two-Step RT-PCR approaches. J. Clin. Virol. *30*, 297–301.

Peacock, T.P., Penrice-Randal, R., Hiscox, J.A., and Barclay, W.S. (2021). SARS-CoV-2 one year on: evidence for ongoing viral adaptation. J. Gen. Virol. *102*, 001584.

Pennings, J., de Locht, L.V., Jansen, J., der Reijden, B.V., Witte, T.D., and Mensink, E. (2001). Degradable dU-based DNA template as a standard in real-time PCR quantitation. Leukemia *15*, 1962–1965.

Piaggio, D., Castaldo, R., Cinelli, M., Cinelli, S., Maccaro, A., and Pecchia, L. (2021). A framework for designing medical devices resilient to low-resource settings. Global. Health *17*, 64.

Qian, C., Wang, R., Wu, H., Zhang, F., Wu, J., and Wang, L. (2019). Uracil-mediated new photospacer-adjacent motif of Cas12a to realize visualized DNA detection at the single-copy level free from contamination. Anal Chem. *91*, 11362–11366.

Ravina, M., Mohan, H., Narang, J., Pundir, S., and Pundir, C.S. (2021). A changing trend in diagnostic methods of Influenza A (H3N2) virus in human: a review. 3 Biotech. *11*, 87.

Roser M. and Ortiz-Ospina E. (2021) – "COVID-19 Data Explorer". Published online at OurWorldInData.org. Retrieved from: 'https://ourworldindata.org/explorers/coronavirus-data-explorer'.

Rubin, R., Abbasi, J., and Voelker, R. (2020). Latin America and its global partners toil to procure medical supplies as COVID-19 pushes the region to its limit. JAMA *324*, 217–219.

Schneider, C., Rasband, W., and Eliceiri, K. (2012). NIH Image to ImageJ: 25 years of image analysis. Nature Methods *9*, 671–675.

Sherrill-Mix, S., Hwang, Y., Roche, A.M., Glascock, A., Weiss, S.R., Li, Y., Haddad, L., Deraska, P., Monahan, C., Kromer, A., et al. (2021). Detection of SARS-CoV-2 RNA using RT-LAMP and molecular beacons. Genome Biol. *22*, 169.

Silva, S.J.R.da, Paiva, M.H.S., Guedes, D.R.D., Krokovsky, L., de Melo, F.L., da Silva, M.A.L., da Silva, A., Ayres, C.F.J., and Pena, L.J. (2019). Development and validation of reverse transcription loop-mediated isothermal amplification (RT-LAMP) for rapid detection of ZIKV in mosquito samples from Brazil. Sci. Rep. UK *9*, 4494.

Stites, E.C., and Wilen, C.B. (2020). the interpretation of SARS-CoV-2 diagnostic tests. Med *1*, 78–89.

Sun, Y., Yu, L., Liu, C., Ye, S., Chen, W., Li, D., and Huang, W. (2021). One-tube SARS-CoV-2 detection platform based on RT-RPA and CRISPR/Cas12a. J. Transl. Med. *19*, 74.

Tsou, J.-H., Leng, Q., and Jiang, F. (2019). A CRISPR test for detection of Circulating nuclei acids. Transl. Oncol. *12*, 1566–1573.

Untergasser, A., Cutcutache, I., Koressaar, T., Ye, J., Faircloth, B.C., Remm, M., and Rozen, S.G. (2012). Primer3—new capabilities and interfaces. Nucleic Acids Res. *40*, e115.

U.S. Centers for Medicare & Medicaid Services (2020). Clinical Laboratory Improvement Amendments (CLIA): CLIA University Lab Testing (PDF) (U.S. Centers for Medicare & Medicaid Services), p. 1.

US Food and Drug Administration. (2014). Framework for Regulatory Oversight of Laboratory Developed Tests (LDTs) (Services UHaH).

US Food and Drug Administration. (2021). Emergency Use Authorization.

Vandenberg, O., Martiny, D., Rochas, O., van Belkum, A., and Kozlakidis, Z. (2021). Considerations for diagnostic COVID-19 tests. Nat. Rev. Microbiol. *19*, 171–183.

Wacker, M.J., and Godard, M.P. (2005). Analysis of one-step and two-step real-time RT-PCR using SuperScript III. J. Biomol. Tech. *16*, 266–271.

Wang, X., Zhong, M., Liu, Y., Ma, P., Dang, L., Meng, Q., Wan, W., Ma, X., Liu, J., Yang, G., et al. (2020). Rapid and sensitive detection of COVID-19 using CRISPR/Cas12a-based detection with naked eye readout, CRISPR/Cas12a-NER. Sci. Bull. *65*, 1436–1439.

WHO (2021). Weekly operational update on COVID-19 - 1 March 2021. https://www.who.int/publications/m/item/weekly-operational-update-on-covid-19—1-march-2021.

Woo, C.H., Jang, S., Shin, G., Jung, G.Y., and Lee, J.W. (2020). Sensitive fluorescence detection of SARS-CoV-2 RNA in clinical samples via one-pot isothermal ligation and transcription. Nat. Biomed. Eng. *4*, 1168–1179.

World Health Organization. (2021). Dos and Don'ts for Molecular Testing.https://www.who.int/teams/global-malaria-programme/case-management/diagnosis/nucleic-acid-amplification-based-diagnostics/dos-and-don-ts-for-molecular-testing.

Xiong, D., Dai, W., Gong, J., Li, G., Liu, N., Wu, W., Pan, J., Chen, C., Jiao, Y., Deng, H., et al. (2020). Rapid detection of SARS-CoV-2 with CRISPR-Cas12a. PLoS Biol. *18*, e3000978.

Zetsche, B., Gootenberg, J.S., Abudayyeh, O.O., Slaymaker, I.M., Makarova, K.S., Essletzbichler, P., Volz, S.E., Joung, J., van der Oost, J., Regev, A., et al. (2015). Cpf1 is a single RNA-guided endonuclease of a class 2 CRISPR-cas system. Cell *163*, 759–771.

Please cite this article in press as: Alcántara et al., Unlocking SARS-CoV-2 detection in low- and middle-income countries, Cell Reports Methods (2021), https://doi.org/10.1016/j.crmeth.2021.100093

STAR★METHODS

KEY RESOURCES TABLE

REAGENT or RESOURCE	SOURCE	IDENTIFIER
Bacterial and virus strains		
E.coli BL21(DE3)pLysS	Promega	Cat # L1195
Biological samples		
Nasopharyngeal swabs	Instituto de Investigación Nutricional, Lima, Peru	N/A
Quantitative PCR (qPCR) control RNA from heat-inactivated SARS-CoV-2, Isolate USA-WA1/2020	Centers for Disease Control and Prevention	BEI Resources NR-52347
Chemicals, peptides, and recombinant proteins		
Ampicilin	Calbiochem	Cat # 171254-56m
Chloramphenicol	Sigma-Aldrich	Cat # C0378-25G
Kanamycin	Sigma-Aldrich	Cat # K1876-25G
Isopropyl ß-D-1 thiogalactopyranoside	ThermoFisher	Cat # R0392
HEPES	Merck Millipore	Cat # 391338-1KG
Ammonium acetate	Supelco	Cat # 101116
Potassium chloride	Supelco	Cat # 104936
Magnesium chloride hexahydrate	Supelco	Cat # 105833
ß-mercaptoethanol	Merck Millipore	Cat # 444203
Lysozyme	PanReac Applichem	Cat # A3711
Trehalose	Sigma-Aldrich	Cat # T9449-25G
cOmplete® Protease Inhibitor Cocktail	Sigma-Aldrich	Cat # 11697498001
Sodium chloride	Supelco	Cat # 106404
Imidazole	Sigma-Aldrich	Cat # I0125
Glycerol 85%	Supelco	Cat # 104094
EDTA	Merck Millipore	Cat # 324503
Tris, Hydrochloride, Molecular Biology Grade	Merck Millipore	Cat # US1648317
Tris base ULTROL grade	Calbiochem	Cat # 643811
Dithiothreitol (DTT)	ThermoFisher	Cat # R0682
dNTP Mix (10 mM each)	ThermoFisher	Cat # R0194
SafeGreen	abm	Cat # G108-G
TriTrack DNA loading dye 6X	ThermoFisher	Cat # R1161
Agarose powder	Cleaver Scientific	Cat # CSL-AG500
Polyacrylamide (40% acrylamide and bis-acrylamide)	Merck Millipore	Cat # 1006381000
OnmiPur Water DEPC treated, sterile, nuclease-free	Sigma-Aldrich	Cat # 9610-1L
DNaseI	PanReac Applichem	Cat # A3778
Unstained Protein Standard, Broad Range (10-200 kDa) ladder	New England Biolabs	Cat # P7717S
AmpliSize Molecular Ruler	Biorad	Cat # 1708200
GeneRuler 100 bp DNA Ladder	Thermo Scientific	Cat # SM0242
Unstained Protein Molecular Weight Marker (14.4 – 116 kDa) ladder	Thermo Scientific	Cat # 26610
Bovine Serum Albumin, lyophilized powder	Sigma-Aldrich	Cat # A9418-100G
Critical commercial assays		
Mix&Go! *E. coli* transformation kit	Zymo Research	Cat # T3002
TranscriptAid T7 High Yield Transcription Kit	ThermoFisher	Cat # K0441

(*Continued on next page*)

Continued

REAGENT or RESOURCE	SOURCE	IDENTIFIER
Direct-zol RNA Miniprep	Zymo Research	Cat # R2051
2X One-Step RT-PCR Master Mix	Norgen BioTek	Cat # 28113
RealTime ready RNA Virus Master	Roche Diagnostics	Cat # 05992877001
Oligonucleotides		
dsDNA oligo: crRNA sequence N target SARS-CoV-2 TAATACGACTCACTATAGGTAATTTCTACTAAGTGTAGATCCCCCAGCGCTTCAGCGTTC	Broughton et al.,2020	N/A
dsDNA oligo: crRNA sequence ORF1ab target SARS-CoV-2 TAATACGACTCACTATAGGTAATTTCTACTAAGTGTAGATTTAGAGACGGTTGGGAAATTG	This paper	N/A
dsDNA oligo: crRNA sequence RNaseP target human sample control TAATACGACTCACTATAGGTAATTTCTACTAAGTGTAGATAATTACTTGGGTGTGACCCT	Broughton et al.,2020	N/A
ssDNA oligo: primer forward N target SARS-CoV-2 TACAAACATTGGCCGCAAATTGC	This paper	N/A
ssDNA oligo: primer reverse N target SARS-CoV-2 CCAATGCGCGACATTCCG	This paper	N/A
ssDNA oligo: primer forward ORF1ab target SARS-CoV-2 GTTGTTCAGTTGACTTCGC	This paper	N/A
ssDNA oligo: primer reverse ORf1ab target SARS-CoV-2 GACAATTTCACAAGCACAGG	This paper	N/A
ssDNA oligo: primer forward RNaseP target human sample control ACTCAGCCATCCACATCC	This paper	N/A
ssDNA oligo: primer reverse RNaseP target human sample control CACCCTCAATGCAGAGTC	Broughton et al.,2020	N/A
reporter_FQ: /56-FAM/TTATT/3IABkFQ/	Chen et al. 2018	N/A
dsDNA templates, see Table S1	This paper	N/A
Recombinant DNA		
pRK793 plasmid	Kapust et al., 2001	Addgene plasmid # 8827; RRID: Addgene_8827
pMBP-LbCas12a Plasmid	Chen et al., 2018	Addgene plasmid # 113431; RRID: Addgene_113431
pET-28a_6H-MMLV_RT_D524N_-6H	Graham et al., 2021	https://gitlab.com/tjian-darzacq-lab/bearmix
pET-28a_6H-TAQ_E602D	Graham et al., 2021	https://gitlab.com/tjian-darzacq-lab/bearmix
Software and algorithms		
ImageJ	Schneider et al., 2012	https://imagej.nih.gov/ij/
GraphPad Prism version 9	GraphPad Software, La Jolla, CA	www.graphpad.com
Stata v14.0	StataCorp, College Station, TX	https://www.stata.com/
Other		
PodSwab™ with UTM™ medium	COPAN	Cat # 3C062N
0.45 μM filter	Merck	Cat # 10418024
HisTrap FF Crude	Cytiva	Cat # 11000458
HiTrap SP Sepharose FF	Cytiva	Cat # 17505401
HiTrap Capto SP ImpRes	Cytiva	Cat # 17546851
MBPTrap HP	Cytiva	Cat # 28918778
D-Tube™ Dialyzer Maxi	Merck	Cat # 71510
96-well flat clear bottom black polystyrene TC-treated microplates	Corning®	Cat # 3603
NanoDrop One microvolume UV-Vis spectrophotometer	Thermo Fisher	Cat # ND-ONE-W
safeVIEW: LED/Blue Light Transilluminator	Cleaver Scientific	Cat # SAFEVIEW

(*Continued on next page*)

Continued

REAGENT or RESOURCE	SOURCE	IDENTIFIER
AkTA™ Start	Cytiva	N/A
Cytation™ 5 Cell Imaging Multi-Mode Reader	BioTek Instruments	N/A
SynergyTM H1 Hybrid Multi-Mode Reader	BioTek Instruments	N/A
Cobas Z480 System	Roche Diagnostics	N/A

RESOURCE AVAILABILITY

Lead contact

Materials and information can be asked to Pohl Milón (pmilon@upc.edu.pe)

Materials availability

The sequences of all generated materials are provided in the article or in Supplemental Information.

Data and code availability

- The published article includes all datasets generated or analyzed during this study.
- This study did not generate/analyze code.
- Any additional information required to reanalyze the data reported in this paper is available from the lead contact upon request.

EXPERIMENTAL MODEL AND SUBJECT DETAILS

Microbes

E.coli BL21(DE3)pLysS cells were cultivated in Luria - Bertani medium.

Nasopharyngeal swabs collection

One hundred nasopharyngeal swabs of hospitalized patients were obtained during the COVID-19 pandemic in 2020. All patient information was anonymized and no sex, nor gender identity were used as study inclusion criteria since the samples were obtained in the context of the epidemiological surveillance emergency program according to the health directives of the National Center for Epidemiology, Disease Control and Prevention of the Ministry of Health of Peru. The study protocol was approved by the Research Ethics Board of the Instituto de Investigación Nutricional, Lima, Peru (N° 395-2020/CIEI-IIN) and by the Ethics Committee of the Universidad Peruana de Ciencias Aplicadas (N° FCS-CEI/187-07-20). All methods were performed in accordance with the relevant guidelines and regulations. The need of an explicit informed consent was waived by the Research Ethics Board of the Instituto de Investigación Nutricional, Lima, Peru. Sample size was calculated with Epidat v4.2. A samples size of N=100 upper-respiratory samples was obtained for a paired-comparative diagnostic test study considering at least a 97% sensitivity for RT-qPCR (gold standard), 78% sensitivity for our molecular toolkit (from a pilot trial), a power level of 80%, a confidence of 95% and a sample size ratio of 1:1.

METHOD DETAILS

Protein expression and purification

Plasmids coding for M-MLV reverse transcriptase (RT) and Taq DNA polymerase, as part of the BEARmix project, were obtained from the Tjian-Darzacq laboratory (https://gitlab.com/tjian-darzacq-lab/bearmix) (Graham et al., 2021). Both proteins are fused with an N-terminal His-tag. Plasmids coding for full-length LbCas12a (#113431) (Chen et al., 2018) and TEV protease S219V (#8827) (Kapust et al., 2001) were obtained from Addgene. Both LbCas12a and TEV protease are fused with an N-terminal His-tag, maltose binding protein (MBP) and TEV protease cleavage site. Plasmids were transformed independently into chemically competent BL21(DE3) *E. coli* using the Mix&Go *E. coli* transformation kit (Zymo Research).

For the M-MLV RT, a single colony was inoculated into Luria-Bertani (LB) medium supplemented with 30 μg/mL kanamycin (Kan) and 17 μg/mL chloramphenicol (Cam) and incubated at 37°C and 150 rpm overnight. The starter culture was subsequently used to inoculate fresh LB medium (+ 30 μg/ml Kan and 17 μg/mL Cam) cultures to an optical density of 0.05 measured at a wavelength of 600 nm (OD600 = 0.05) and grown at 37°C and 150 rpm until cells reached OD600 = 0.8. Protein expression was induced with 1 mM isopropyl β-d-1-thiogalactopyranoside (IPTG) at 37°C for 3 h with agitation at 150 rpm. Cell pellets were harvested and washed with TAKM buffer (50 mM Tris-HCl pH 7.4, 70 mM NH_4Ac_2, 30 mM KCl, 10 mM $MgCl_2$) by centrifugation at 5 000 rpm and 4°C for 5 min. After that, cell pellets were harvested again and resuspended in MB1 (50 mM Tris-HCl pH 8, 100 mM NaCl, 10 mM imidazole, 6 mM

β-mercaptoethanol, 0.1% Tween 20) with 100 μg/mL lysozyme, 40 μg/mL DNase I, 10 mM $MgCl_2$ + Complete protease inhibitor (Roche) and stored at −80°C.

Cells were lysed by two freeze/thaw cycles and NaCl concentration was fixed to 370 mM. The lysate was centrifuged at 10 000 rpm and 4°C for 45 min. The supernatant was filtered through a 0.45-μm Millex-HV syringe filter (Sigma-Aldrich) and manually loaded onto a 1 mL Column Volume (CV) HisTrap FF Crude column, pre-equilibrated with MB1. The column was washed twice with MB2 (50 mM Tris-HCl pH 8, 500 mM NaCl, 10 mM imidazole, 6 mM β-mercaptoethanol, 0.1% Tween 20) and MB1. The protein was eluted with 250 mM imidazole in MB3 (50 mM Tris-HCl pH 8, 100 mM NaCl, 250 mM imidazole, 6 mM β-mercaptoethanol, 0.1% Tween 20). Fractions were analyzed by 10% SDS-PAGE and the relevant fractions containing protein were pooled and dialyzed overnight at 4°C against MB4 (50 mM Tris HCl pH 8, 100 mM NaCl, 0.1 mM EDTA, 6 mM β-mercaptoethanol, 0.1% Tween 20). The protein was loaded onto a 1 mL HiTrap SP column pre-equilibrated with MB4 and washed twice with the same buffer. M-MLV RT was eluted with linear gradient using MB4 (100 mM NaCl) and MB5 (50 mM Tris-HCl pH 8, 1 M NaCl, 0.1 mM EDTA, 6 mM β-mercaptoethanol, 0.1% Tween 20) in 20 CVs, analyzed by 10% SDS-PAGE, pooled and dialyzed in MB6 (50 mM Tris HCl pH 8, 100 mM NaCl, 0.1 mM EDTA, 1 mM DTT (added just before use), 0.1% Tween 20 or Triton X-100, 50% glycerol).

For the Taq DNA polymerase, cellular expression was done as described before for M-MLV RT. Cell pellets were also harvested and washed with TAKM buffer. After that, cell pellets were stored resuspended in TaB1 (50 mM Tris HCl pH 8, 500 mM NaCl, 0.1% NP-40 and 0.1% Triton X-100) with 100 μg/mL lysozyme, 40 μg/mL DNase I, 10 mM $MgCl_2$ + Complete protease inhibitor (Roche) at -80°C. Cells were lysed by two freeze/thaw cycles and heated at 80°C for one hour. The lysate was centrifuged at 10 000 rpm and 4°C for 45 min and the buffer was fixed to 6 mM β-mercaptoethanol, 10 mM imidazole, 10% glycerol. The supernatant was filtered and manually loaded onto a 1 mL HisTrap FF Crude column that was pre-equilibrated with TaB1. The column was washed with TaB2 (50 mM Tris HCl pH 8, 500 mM NaCl, 0.05% NP-40, 5% glycerol, 10 mM imidazole, 6 mM β-mercaptoethanol) and TaB3 (50 mM Tris HCl pH 8, 100 mM NaCl, 0.05% NP-40, 5% glycerol, 10 mM imidazole, 6 mM β-mercaptoethanol), and eluted with TaB4 (TaB3 buffer containing 300 mM imidazole). Fractions were analyzed by 10% SDS-PAGE and relevant fractions containing the protein were pooled and dialyzed overnight at 4°C against TaB5 (50 mM Tris HCl pH 8, 100 mM NaCl, 0.05% NP-40, 10% glycerol, 6 mM β-mercaptoethanol). Pooled fractions were loaded onto a 1 mL HiTrap Heparin HP column and washed twice with TaB5. Fractions were eluted with a salt gradient up to 1 M NaCl with TaB6 (TaB5 containing 1 M NaCl), analyzed by 10% SDS-PAGE, pooled and dialyzed in TaB7 (50 mM Tris HCl pH 8, 100 mM NaCl, 0.1 mM EDTA, 1 mM DTT, 50% glycerol).

For the TEV protease, a single colony was inoculated into LB medium supplemented with 100 μg/mL ampicillin (Amp) and 30 μg/mL Cam and incubated at 37°C and 150 rpm overnight. The starter culture was subsequently used to inoculate fresh LB medium (+ 100 μg/mL Amp and 30 μg/mL Cam) cultures to an OD600 = 0.05 and grown at 37°C and 150 rpm until cells reached OD600 = 0.5. Protein expression was induced with 1 mM IPTG at 30°C and 150 rpm for 3 h. Cell pellets were harvested by centrifugation at 5 000 rpm and 4°C for 10 min and resuspended in $HAKM_{10}$ buffer (50 mM HEPES pH 7.4, 70 mM NH_4AC, 50 mM KCl, 10 mM $MgCl_2$, 6 mM β-mercaptoethanol). Then, 100 μg/mL lysozyme and Complete Protease Inhibitor Cocktail (1 tablet/25 mL) (Roche) were added to the cell suspension, mixed and stored at -80°C. Cells were lysed by two freeze/thaw cycles in the presence of 40 μg/mL DNase I. The lysate was centrifuged at 10 000 rpm and 4°C for 45 min. The supernatant was filtered through a 0.45-μm Millex-HV syringe filter (Sigma-Aldrich) and manually loaded onto a 1 mL HisTrap FF Crude column that was pre-equilibrated with TeB2 (20 mM HEPES pH 7.4, 300 mM NaCl, 6 mM β-mercaptoethanol containing 10 mM imidazole). The column was washed with TeB3 (50 mM HEPES pH 7.4, 300 mM NaCl, 50 mM imidazol, 6 mM β-mercaptoethanol) and eluted with TeB4 (50 mM HEPES pH 7.4, 300 mM NaCl, 100 mM imidazole, 6 mM β-mercaptoethanol). Eluted fractions were analyzed by 12.5% SDS-PAGE and Coomassie blue staining. Fractions containing the TEV protease were pooled and dialyzed overnight at 4°C against TeB5 (25 mM HEPES pH 8.0, 200 mM NaCl, 20% glycerol, 1 mM ethylenediaminetetraacetic acid (EDTA), 6 mM β-mercaptoethanol) using a D-Tube™ Dialyzer Maxi, MWCO 12-14 kDa (Sigma-Aldrich).

For LbCas12a, a single colony was inoculated into LB medium supplemented with 100 μg/mL Amp and incubated at 37°C and 150 rpm overnight. The culture was diluted in fresh LB medium (+ 100 μg/mL Amp) and grown at 37°C and 150 rpm until OD600 of 0.5 was reached. The cultures were incubated on ice for 15 min before induction with 0.2 mM IPTG at room temperature and 150 rpm overnight. Cell pellets were harvested by centrifugation at 5000 rpm and 4°C for 10 min, resuspended in HAKM buffer with 400 mM NaCl, 100 μg/mL lysozyme, 40 μg/mL DNase I + Complete protease inhibitor (Roche) and stored at -80°C. The cell pellet was lysed by 2 freeze/thaw cycles. The lysate was centrifuged at 10000 rpm and 4°C for 45 min. The supernatant was filtered through a 0.45-μm Millex-HV syringe filter (Sigma-Aldrich) and loaded onto a 1 mL HisTrap FF Crude column that was pre-equilibrated with CB1 buffer (20 mM HEPES pH 7.4, 300 mM NaCl, 10 mM imidazole, 6 mM β-mercaptoethanol). The protein was washed with CB2 (50 mM HEPES pH 8, 300 mM NaCl, 50 mM imidazole, 6 mM β-mercaptoethanol) and CB3 (50 mM HEPES pH 8, 300 mM NaCl, 100 mM imidazole, 6 mM β-mercaptoethanol) and eluted with CB4 (50 mM HEPES pH 8, 300 mM NaCl, 250 mM imidazole, 6 mM β-mercaptoethanol). Eluted fractions were analyzed by 7.5% SDS-PAGE and Coomassie blue staining. Fractions containing LbCas12a were pooled and TEV protease was added to 2.21 μM final concentration. The sample was dialyzed overnight at 4°C against CB5 (25 mM HEPES pH 7.5, 200 mM NaCl, 20% glycerol, 1 mM EDTA, 6 mM β-mercaptoethanol) using a D-Tube™ Dialyzer Maxi, MWCO 12-14 kDa (Sigma-Aldrich).

For further purification, the dialyzed sample was manually loaded onto a 1 mL MBPTrap HP column that was pre-equilibrated with CB6 (20 mM HEPES pH 7.5, 125 mM KCl, 5% glycerol, 1 mM β-mercaptoethanol). The flow through (FT) with the protein was collected and the remaining MBP trapped in the column was washed with CB7 (20 mM HEPES pH 7.5, 125 mM KCl, 5% glycerol,

6 mM β-mercaptoethanol, 10 mM maltose), CB6 and stored as recommended by the producer. Following, the FT was loaded in a 1 mL HiTrap SP HP column pre-equilibrated with CB6. LbCas12a was washed with CB6 and eluted with CB8 buffer (20 mM Tris-HCl pH 7.5, 200 mM NaCl, 20% glycerol, 1 mM DTT, KCl linear gradient). Recollected fractions were visualized by 7.5% SDS-PAGE and Coomassie blue staining. Fractions containing the LbCas12a protein were pooled and concentrated with an Amicon Ultra-4, membrane PLQK Ultracel-PL, 50 kDa (Sigma-Aldrich). The sample was then dialyzed overnight at 4°C against CB8 using a D-Tube™ Dialyzer Maxi, MWCO 12-14 kDa (Sigma-Aldrich).

Dialyzed proteins, M-MLV RT, Taq DNA polymerase and TEV protease were aliquoted and stored at -20°C, LbCas12a was stored at -80°C. Protein concentrations were determined by the Bradford assay using bovine serum albumin (BSA) for the standard curve.

crRNAs preparation

crRNAs were prepared from synthetic dsDNA templates (100 pmoles) using TranscriptAid T7 High Yield Transcription Kit (Thermo Fisher Scientific) at 37°C for 3 h. Immediately thereafter, crRNAs were purified using Direct-zol RNA miniprep (Zymo Research) with a DNase I (30 U) digestion in a column step for 15 min at room temperature and eluted in nuclease-free water. Finally, crRNAs were quantified by NanoDrop One microvolume UV-Vis spectrophotometer (Thermo Fisher Scientific), aliquoted to working volumes and stored at -80 °C.

RT-PCR assays

The RT-PCR assay was standardized using pooled patient samples with high viral load (Cq < 30) and low viral load (Cq > 31), and non-template reactions as negative controls. Sample pools were prepared by mixing 10 high viral load and 10 low viral load samples, respectively. Initial conditions were based on reported data (Graham et al., 2021). Master mix reactions were prepared using the enzymes M-MLV RT and Taq DNA polymerase, produced as described above. RT-PCR products were visualized in 5% agarose gel as described above.

In order to find optimal conditions, one-step and two-step RT-PCR reactions were compared. Additionally, reverse transcription time (10 and 20 minutes), different sample volumes (0.5, 1, 2, and 4 μL), different concentrations of Taq DNA polymerase (0.8 ng/μL, 1.6 ng/μL, 3.2 ng/μL, 8 ng/μL, and 16 ng/μL) and of M-MLV RT (0.8 ng/μL, 1.7 ng/μL, 3.4 ng/μL, and 5.1 ng/μL) were evaluated. Enzyme dilutions were prepared in MB6 buffer. The analytical sensitivity was evaluated using a range of SARS-CoV-2 genomic RNA (NR-52347, BEI Resources) between 10^4 and 1 viral genome equivalents (ge) per microliter of reaction. Additionally, the analytical sensitivity of the RT-PCR was compared with that of a commercial 2X One-Step RT-PCR Master Mix (Norgen BioTek) for the N target. The amplified products were verified by 5% agarose gel electrophoresis (TBE 1X, 70V for 45 minutes), and visualized using Safe-Green (N° Cat. G108-G, abm) in the loading buffer TriTrack DNA loading dye 6X (N° Cat. R1161, ThermoFisher) in a safeVIEW: LED/Blue Light transilluminator (Cleaver Scientific).

The optimized conditions of SARS-CoV-2 RNA amplification by RT-PCR used a 20 μL RT-PCR reaction with 1.6 ng/μL of Taq DNA polymerase, 1.7 ng/μL M-MLV RT, 0.4 mM dNTPs and 0.2 μM of each primer in RPB1X (50 mM Tris-HCl, 75 mM KCl, 3 mM $MgCl_2$, 10% trehalose, 10 mM DTT, 0.1 mM EDTA, pH 8.4, 25°C) with 2 μL of RNA sample. The reaction used a reverse transcription step at 50°C for 20 minutes, followed by an initial denaturation at 95°C for 5 minutes, and 45 cycles of denaturation at 95°C for 3 seconds and a single annealing-extension step at 55°C for 30 seconds.

CRISPR-Cas12a *trans*-cleavage assays

The CRISPR-Cas12a-based assays were standardized using synthetic dsDNA as templates in 96-well flat clear bottom black polystyrene tissue culture-treated microplates (Corning). Reporter probe (/56FAM/TTATT/3IABkFQ/, Macrogen) (Chen et al., 2018), recombinantly purified LbCas12a and *in vitro* transcribed crRNAs, prepared as described above, were used in all assays. CrB1X buffer (50 mM NaCl, 10 mM Tris-HCl, 100 μg/ml BSA, pH 7.9, 25°C) + 15 mM $MgCl_2$ was used for all steps, unless differently specified in the text or figure legends.

Initial settings were based on previous reports (Broughton et al., 2020; Chen et al., 2018). For each test, the crRNA was first refolded at 65°C for 10 min in a heating block followed by slow cooling for 10 minutes at room temperature to enhance homogeneous folding. Afterward, the Cas12a:crRNA:reporter complex was formed for 10 min at room temperature. Each CRISPR-Cas12a assay consisted of 10 nM Cas12a and 15 nM crRNA using 0.3 μM reporter. Different concentrations of Cas12a (5 nM, 10 nM, 25 nM and 50 nM), crRNA (5 nM, 10 nM, 15 nM, 25 nM, 50 nM, 75 nM, 100 nM), and $MgCl_2$ (2.5 mM, 5 mM, 10 mM, 15 mM, 20 mM) were tested to find optimal conditions. The analytical sensitivity was evaluated using a range of synthetic dsDNA template concentrations between 1 pM and 10 nM. Standardization assays were performed independently for both SARS-CoV-2 N and ORF1ab targets, and the human RNase P control template.

The optimized conditions of CRISPR/Cas12a assays used five microliters of unpurified RT-PCR products diluted in 85 μL of CrB1X (50 mM NaCl, 10 mM Tris-HCl, 100 μg/mL BSA, pH 7.9, 25°C) + 15 mM $MgCl_2$. Briefly, the Cas12a:crRNA:reporter complex was prepared at 10X concentration (100 nM Cas12a, 150 nM crRNA, 3 μM reporter probe) in CrB1X. Ten microliters of the 10X Cas12a:crRNA:reporter complex were mixed with 90 μL of the diluted RT-PCR products in a final volume of 100 μL to start the reaction. Kinetic assays monitored fluorescence signal at an excitation wavelength of 491±9 nm and an emission wavelength of 525±24 nm every minute for 2 h at room temperature using a fluorescence plate reader (Cytation™ 5, BioTek Instruments).

Fluorescence ratios (test sample fluorescence over that of RT-PCR non template control (NTC)) were used for analysis. Initial velocity (V_0) was estimated using linear regression of the fluorescence time courses.

End-point CRISPR-Cas12a assays

For end-point CRISPR-Cas12a assays, SARS-CoV-2 N and ORF1ab targets and the human RNAseP control were amplified from clinical samples with confirmed SARS-CoV-2 infection status. Two clinical samples each with high, medium, and low viral RNA load, as well as two negative (SARS-CoV-2 not detected) samples were evaluated using a conventional T-100 thermal cycler (Bio-Rad) and the mobile molecular equipment BentoLab (https://www.bento.bio/). Thermocycler and gel electrophoresis/transilluminator modules of the portable BentoLab were used for RT-PCR, agarose gel visualization and CRISPR-Cas12a-based direct tube detection. RT-PCR and CRISPR-Cas12a reactions were performed as previously described. The fluorescence readout was monitored by naked-eye visualization every 5 min during 1 h in a safeVIEW: LED/Blue Light transilluminator (Cleaver Scientific) and the electrophoresis/transilluminator module of the portable lab using a Black Box adaptation.

Clinical samples and validation

Nasopharyngeal swab samples were collected using COPAN swabs and UTM medium. The viral genetic material was extracted using the QIAamp viral RNA Mini Kit (250) (Cat N° 52906, QIAGEN) to perform the RNA extraction from 200 μL of the samples, according to the manufacturer's instructions. Viral RNA obtained after the extraction was eluted in 100 μl of nuclease-free water. For this study, a double-blind approach was used with 50 positive and 50 negative samples for SARS-CoV-2. The gold standard detection used the amplification of SARS-CoV-2 using Real Time ready RNA Virus Master and 250 nM specific primers for SARS-CoV-2: gene E, gene RdRP (RNA-dependent RNA polymerase) and gene N (Roche Diagnostic). The qPCR reactions and analysis were performed according to the manufacturer's instructions. All procedures were performed using the Cobas Z480 System (Roche Diagnostic).The reference RT-qPCR test provided the quantification cycle (Cq, equivalent to the cycle threshold (Ct)), which is a semi-quantitative measure for the viral load, meaning that a low Cq-values indicates high viral RNA load, and a high Cq-value indicates a low viral RNA load. Cq values for the RdRP gene were used to assign RNA load categories.

Bioinformatic analyses

Ninety-six SARS-CoV-2 genomes (as of March 22, 2020) were aligned locally using the ClustalX package for Ubuntu with default parameters (Table S1) (Larkin et al., 2007). Conserved regions were identified with the AliView software (Larsson, 2014). Protospacer adjacent motif (PAM) sequences (TTTV) for LbCas12a were searched to identify 20 nt-long recognition sites. Double-stranded DNA (dsDNA) templates for crRNA generation through *in vitro* transcription were designed with a T7 promoter, followed by the scaffold and the specific recognition site (Table S1). Synthetic dsDNA templates containing the recognition site and flanking regions were designed manually. Primers were designed manually or with the Primer3Plus v.2.4.2 server with the default settings and an average Tm of 56 °C (Untergasser et al., 2012).

QUANTIFICATION AND STATISTICAL ANALYSIS

Data analysis was performed using Prism 9 (GraphPad Software) and STATA v14.0 (StataCorp). Fluorescence signal over time was analyzed by linear regression fitting to determine the initial velocity at varying times (5-30 min). Fluorescence intensity ratios between synthetic template (cognate) and synthetic control (non-cognate) were calculated for each fluorescence reading during CRISPR-Cas12a optimization assays. Similarly, fluorescence intensity ratios between the test sample and RT-PCR non-template control (blank) were calculated for each fluorescence reading during RT-PCR optimization assays and clinical validation. Briefly, the raw fluorescence data were normalized by subtracting the first fluorescence reading. On the basis of the fluorescence ratios obtained, the highest fluorescence ratio was used to identify the best conditions for RT-PCR (one-step or two-step reactions, reverse transcription time, locally produced enzyme concentrations, sample volume), and heatmaps were plotted over time in order to estimate the best conditions for the CRISPR-Cas12a assay (crRNA, Cas12a and $MgCl_2$ concentrations). The limit of detection (LOD) assay was performed in triplicates to calculate mean and SD values. A mean fluorescence of five reading points was used for all fluorescence ratio calculations. If appropriate, the rules of error propagation were applied. Clinical performance parameters such as sensitivity and specificity were calculated based on cutoff values determined by a Receiver Operating Characteristic (ROC) curve analysis (Hanley and McNeil, 1982). Cutoff values with the highest percentage of correctly classified samples were selected for fluorescence ratios and initial velocity for N and ORF1ab targets, independently. The estimated sensitivity and specificity, and the area under the ROC curve with respective 95% confidence intervals (CI) were reported for all samples and within each grouping by viral RNA load levels. Additionally, the average of negative controls plus three-standard deviations was considered for comparisons to cutoff values calculated by the ROC analysis.